# POWER CONVERSION SYSTEM FOR GRID CONNECTED MICRO HYDRO POWER SYSTEM WITH MAXIMUM POWER POINT TRACKING

by

A Thesis Submitted in

Partial Fulfillment of the

Requirements for the Degree of

Master of Science

in Engineering

at

The University of Wisconsin-Milwaukee

May 2017

ABSTRACT

GRID CONNECTED MICRO HYDRO POWER SYSTEM WITH MAXIMUM POWER POINT TRACKING CONTROL
by

Zhuoyu Jiang

The University of Wisconsin-Milwaukee, 2017
Under the Supervision of Dr. Adel Nasiri

This research analyzed and simulated an electrical power conversion system for a grid-connected variable speed micro hydro turbine (MHT) system. Different from traditional hydro power systems, the MHT is running at variable speed condition with permanent magnet synchronous generator(PMSG). To decouple the relationship between the generator rotation speed and the output frequency, rectifier and DC boost converter is developed to maintain the output voltage when the generator is rotating in a low speed. The reference generator speed is given by the perturbation and observation maximum power point algorithm to extract more energy from the micro hydro turbine. The grid connected inverter converts the power from the DC side to the grid with a D-Q frame control. If the generator speed is high enough, the inverter will directly control the generator speed.

TABLE OF CONTENTS

LIST OF FIGURES

LIST OF TABLES

# Chapter 1 Introduction

## 1.1Micro hydropower system

Hydropower is one of the most reliable and developed renewable energy generation for the human being at present. It is also the largest renewable energy source that produces around 16% of the world's electricity and over 80% of the world's renewable electricity. The United States are one of the countries which have the largest hydropower generation capacity. [1]

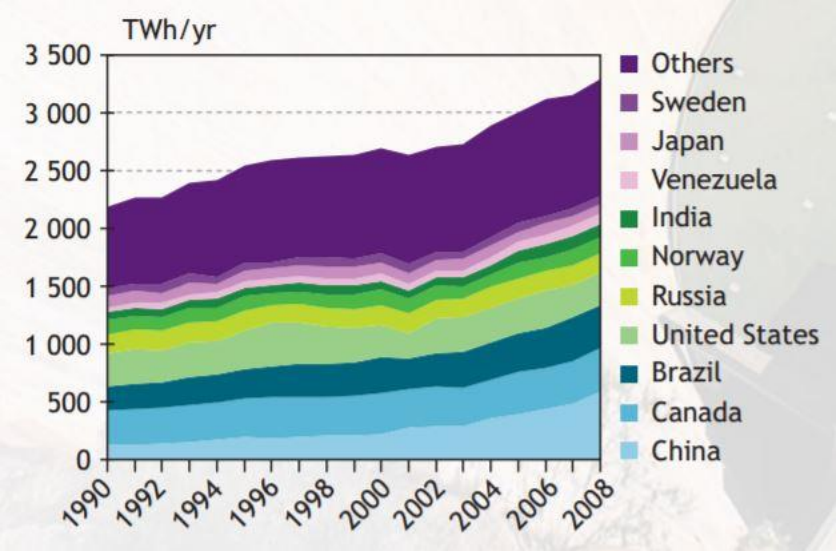


Figure 1-1 World hydropower generation 1990-2008 [1] data source: IEA.

From the figureFigure 1-1 World hydropower generation 1990-2008 [1] data source: IEA, we can see that the total hydropower production increased by 50% since 1990 and reach 3288 TWh in 2008[11]. However, in the United States, the increment of hydropower is not as significant as the increase in other regions.

Hydropower plants are not available for most people to build because electricity generated by hydropower is targeted to be delivered to the vast power network usually rated at 10 megawatts(MW) and a conventional hydropower plant normally associate with large dam construction. However, in recent years, the idea of the microgrid provides people more access to smaller-scale renewable energy. The microgrid is developed for localized electricity generation and distribution. Both of power source or load in a microgrid can be either grid connected or islanded [9].

Because of flexible distribution of the microgrid scheme, hydropower can be scaled to a smaller power rating for better utilization of the local reliable renewable resource. The micro hydropower concept is induced for fully utilizing the renewable energy from the flowing water. Micro-hydropower is typically rating from 5 KW to 100KW. Like other renewable resources in a microgrid, micro hydropower system can either deliver electric power to an isolated load or be connected to the grid [2]. A typical micro hydropower system consists of:

(1) water conveyance: storage sink, pipe or penstock

(2) micro-hydro turbine: transfer mechanical energy

(3) generator and power control system: transfer mechanical energy into electrical energy and deliver the power to the local load or utility grid.

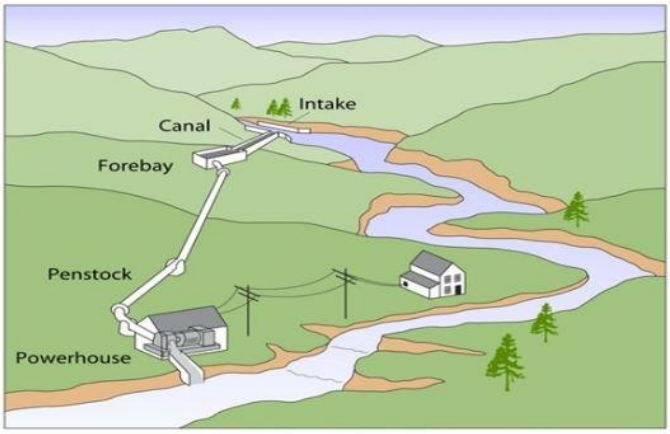


Figure 1-2 Micro hydropower plant overview with penstock [2].

Figure Figure 1-2 Micro hydropower plant overview with penstock [2] shows an overview of the micro hydropower system: the water in a flowing river from the intake is diverted into a canal. It will form a forebay which is a settling tank to hold the flowing water. The penstock or pipe then will lead the water into the mechanical turbine and rotates the shaft. This rotation then will be utilized by the generator to produce electric power that either is used by local loads or is delivered to the electric power network [2].

The power can be accessed from the water is determined by two characters of the water. The first thing is head which is the vertical difference between the front of water conveyance and the turbine. The second point is the flow which is the mass of falling water. The total power in the water is the production of the water head and flow [3].

Such a small-scale hydropower system is suitable for a homeowner and small business owners who have access to the flowing water with a relatively high head (3 feet or above) but located in remote communities. Different from the traditional hydropower plants which are usually built on large dams, micro hydro power systems are usually "run of river" which do not require a dam to cut off the river for power generation. The run of river system allows very short term water storage which provide more flexibility to handle

different load situation. It is more affordable than the traditional hydropower because run-of-river schemes cost much less than a reservoir dam. There is another drawback of large hydropower plants from an environmental point of view that is ecosystem will be dramatically changed because of constructions of dams and hydropower plants. Even though the hydropower source is clean, the environment has already been damaged before the renewable energy is utilized. In California, large hydroelectric facilities greater than 30 megawatts(MW) are not eligible for California's renewable portfolio standards [4]. Compared to the huge total amount of hydro electricity generation, the scale of the micro hydropower plant is almost negligible in the United States. However, in some small country like Nepal, micro hydro power plants are critical for the resident. Around 3300 MHP have been installed in hilly and mountains location in Nepal. These mini/micro hydro power plants are generating close to 30,000 KW of installed capacity to provide electricity for about 350,000 households. Lighting has been the main benefit of MHPs. Grinding, hulling and water pumping is also done with electricity generated by MHPs and also powered to operate computers, photo studios, poultry farms and some small industries [12]. At present, these micro hydro power plants are faced with grid connection challenge. Most of these plants are running in an off-grid mode for local power supply. However, as the Nepal Electricity Authority(NEA), the state-owned electricity utility, extend the grid to those remote areas, many micro hydropower plants need to be redundant if they can't be connected to the grid. If the grid connected requirement is not met, many of the micro hydro power plants are forced to shut down [14].

## 1.2Variable speed generator system

For a traditional hydropower system, the magnitude of the output voltage can be adjusted by transformers to match the grid requirement. However, the rotation speed of a synchronous generator is coupled to the frequency of the grid because transformer can only change the magnitude of the voltage. The frequency difference between the generator and the grid is critical for power delivery. Thus, we do not have the degree of freedom to manipulate the generator speed because it is controlled by the grid frequency. The relationship between the generator speed n and output voltage frequency f is given by the equation:

$$f = n * \frac{p}{120}$$

Where generator rotation speed n is in revolutions per minute(rpm), the frequency f is in hertz and p is the numbers of poles. For a 50Hz grid, generators are usually running at 3000 rpm or 1500 rpm. 3600 rpm and 1800 rpm are typical speed for a 60Hz grid. The fixed speed is named synchronous speed. The output power P of the generator is the product of speed ω and torque τ:

$$P = \omega * \tau$$

Where P is in watt, rotation speed ω is in rad/s, and torque τ is in N/m. Since the generator speed is fixed because of the coupling with the grid frequency, the only parameter that affects the output power is the mechanical torque. However, the synchronous speed is usually not the ideal speed for extracting power from the renewable source. From the equation, we can easily tell that the output power from the turbine will increase if we increase the rotation speed at the same torque input. To optimize the output power from the generator and turbine, it is necessary to decouple the relationship between the output voltage frequency and rotation speed. Thus, the

variable speed generator system is induced to solve this problem. From figure**Error! Reference source not found.**, we can see the area of possible operation speed for different turbine other than the fixed rotation speed if the system is running at variable speed

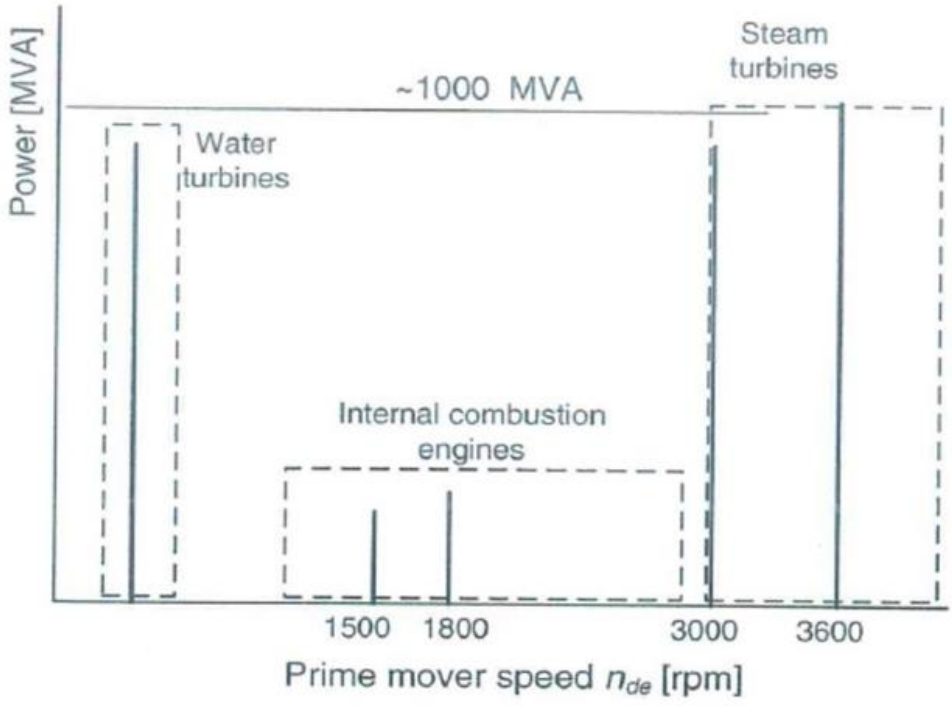


Figure 1-3 Available operation range for water turbine, ICE, and steam turbines.

A typical variable speed generator system is a wind turbine system(WTS) which is similar to the micro hydropower system. According to [5], the mechanical power that the wind turbine can extract from wind energy is:

$$Pm = \frac{1}{2} * \rho * A * Cp * V^3$$

Where ρ is the air density, A is the sweep area of the turbine blades. V is the wind speed, and Cp is the aerodynamic power coefficient. Cp is a function of the pitch angle β and the tip speed ratio(TSR) λ. In this equation, under a certain wind speed, the air density, sweep

area, and wind speed are fixed. The only parameter that affects the output mechanical power is the aerodynamic power coefficient Cp.

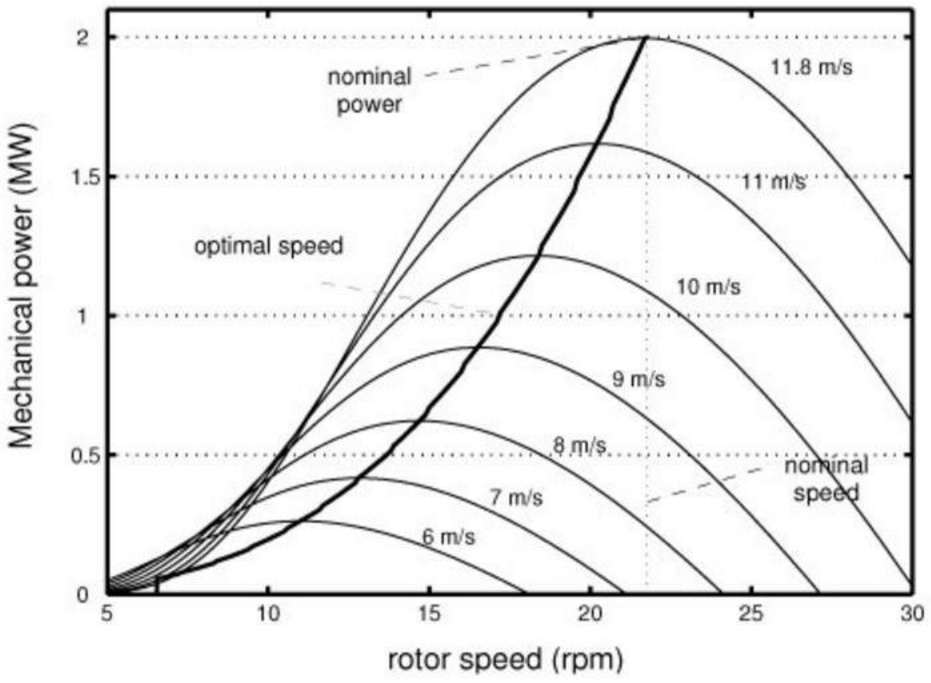


Figure 1-4 Wind turbine optimal speed and nominal power relationship at different wind speed [5].

As we can see from the figure, to keep the wind turbine running at the most efficient Cp, the TSR needs to be maintained at a particular value. TSR is defined by the following equation [5]:

$$\lambda = \frac{\omega * R}{V}$$

Where R is the wind turbine blade radius, ω is the wind turbine speed, and V is the input wind speed. From the equation, the turbine speed needs to be adjusted in real time based on the change of the input wind speed. It can't be achieved by a simple transformer because the traditional transformer has no control of the generator speed or frequency. Thus, the power electronics units are induced for variable generator speed system.

Power converter circuit topologies consist of different types of semiconductors like the diode and insulated gated bipolar transistors(IGBT) with capacitors and inductors. IGBT are the most common switching component in low voltage (690V) voltage source converter (VSC) [16]

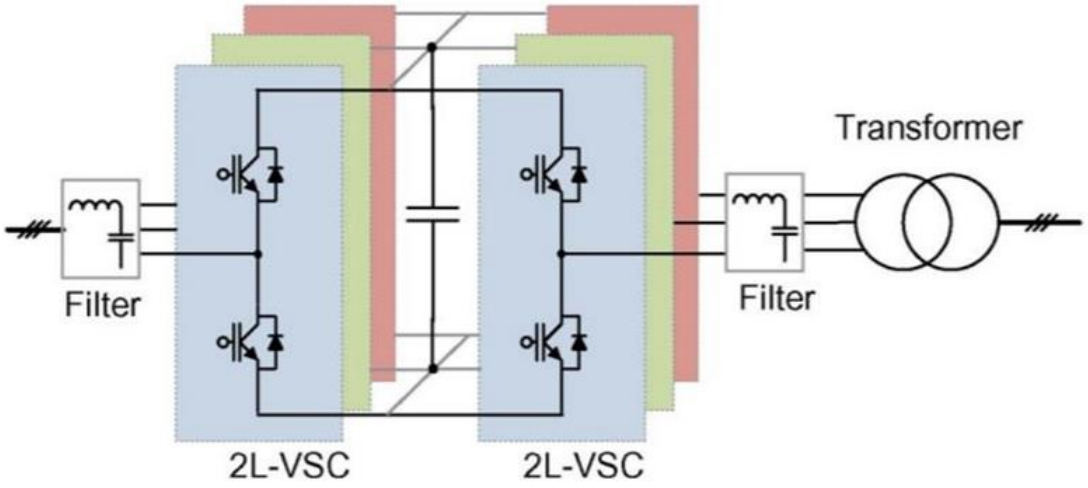


Figure 1-5 Topology of voltage source converter with 2-level output voltage [16].

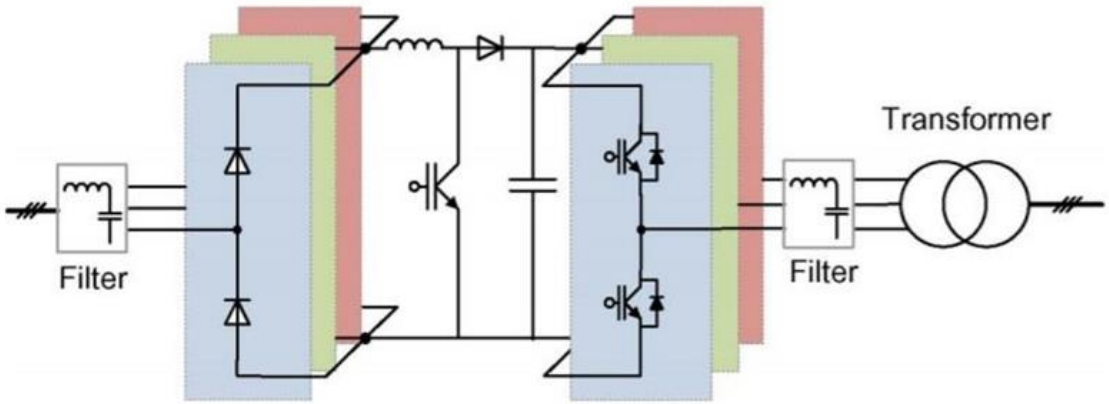


Figure 1-6 Topology of unidirectional power converter with a passive diode and boost converter [16].

Two typical power converter topology are shown in figure1-5 and 1-6. The first topology is called pulse width modulation voltage source converter with two level output

voltage(2L-BTB) [15]. It is widely used in doubly fed induction generator-based system with high robustness and reliability. However, such a topology may suffer from power losses problem because more switches are needed at the generator side control especially in megawatts (MW) levels [15]. The other issue of the 2L-BTB topology is the total harmonic distortion(THD) of voltage. Bulky output filter will probably need to be used on the grid side to reduce the THD and limit the voltage gradient [17]. The second topology is called unidirectional power converter which is frequently used in permanent magnetic synchronous generator(PMSG) based system. In this topology, the three phase full bridge diodes ensure the unidirectional power flow of the system. The boost converter is used to control the generator speed and match up with the DC link voltage [15]. Both of two topologies are single-cell power converter and widely used in variable speed turbine system. The unidirectional power converter will be used in this micro hydropower research because the system is based on the PMSG.

## 1.3Previous work review of the micro hydro power plants

In 1993, D. S. Henderson and D. E. Macpherson presented a novel control method of electronic load governor for a micro hydro generator to balance the generator power production and the user's load requirement [18]. The idea of power electronics components is induced in this research called solid state switching devices. Unlike the traditional speed governors which maintain the generator speed by adjusting the water flow, the paper proposed electronic load governor for speed adjustment. Switching devices are used for switching on or off the ballast load to balance the system. In this

article, the balance is achieved, but specific topology or algorithm of the switching devices was not given.

Some other stand-alone micro hydropower research based on induction generator shared the same idea with D. S. Henderson and D. E. Macpherson that compensate the load differences by manipulating the switching circuit of the ballast load. For example, Nigel P. A. Smith demonstrated three approaches to ballast load which was phase angle control, switched binary-weighted loads and variable mark space ratio chopping [19]. The maximum power point of the hydro turbine was also mentioned in this paper.

Based on the search results on IEEE, many types of research related to the micro hydropower were the stand-alone model, and the induction generator was a favorite kind of generator in the system. More paper focused on micro hydropower with PMSG were published after 2010.

In 2014, D. Melly, R. Horta, C. Münch, H. Biner, S. Chevailler designed two permanent magnet machines along with AC-DC converter for a new axial counter-rotating turbine [20]. The DC bus voltage control is done by a rectifier topology called Vienna rectifier. Such a control strategy has great robustness, high power density, a low blocking voltage stress on power semiconductors and sinusoidal current requirement [21]. By the experimental results of the turbine prototype, it showed a stable control of the system with high efficiency.

Khalid Tourkey Atta, Andreas Johansson, Michel J. Cervantes, and Thomas Gustafsson [22] proposed a maximum power point tracking method for the micro-hydropower turbine. Extremum seeking control is discussed in this paper. It is a single objective optimization concept for dynamic systems. The simulation results of the algorithm were demonstrated,

and the experimental data of the whole system showed the possibility of using this algorithm in the micro hydropower plant. The typical structure of micro hydropower system should use PMSG with an AC/DC/AC power converter as mentioned in their paper. However, the generator utilized in the experiment is a Siemens DC generator which is connected to the grid through a DC converter.

Rakesh C. Prajapati, Dipendra Rai, and Bhupendra B. Chhetri discussed a more relevant aspect of the micro hydropower system [23]. As mentioned above, micro hydro power plants are critical in Nepal electricity generation but are faced with utility connection problem. This paper introduces a novel method for indigenous design and construction of a simple and economic low data rate power line modem. Their low cost but a reliable design of power line modem and construction for the utility applications in micro hydropower system are demonstrated [23].

In the above research papers, none of them present a maximum power point tracking algorithm and control scheme for micro hydro power plant with PMSG

## 1.4Thesis motivation and structure overview

This thesis reviews the topology of the variable speed generator system with a permanent magnetic synchronous generator(PMSG). The mechanically driven turbine is micro-hydropower turbine which does not have a particular accurate model. From the turbine simulation result, a maximum power point clearly exists. To achieve the maximum power output, the observation & perturbation maximum power point tracking algorithm is applied to the system. A micro hydro turbine with PMSG running at variable speed is simulated and validate the control methods.

The first chapter of the thesis introduces the idea of the micro hydropower plants and the real-life application. Also, state of the art topology of variable speed generator system is induced for a more reliable and efficient control of the micro-hydropower turbine.

In the second chapter, the micro hydro turbine will be modeled based on a set of simulation results of a Kaplan hydro turbine. A simplified model equation will be proposed. The permanent magnet synchronous generator model in natural ABC phase and rotational d-q axis will be presented.

In chapter 3, the full bridge three phase diode rectifier and boost converter topology will be given. Small signal analysis of the boost converter for current will be discussed. The speed control of the generator is implemented in boost converter control.

In chapter 4, the inverter model based on pulse width modulator and perturbation & observation algorithm will be introduced. The voltage oriented control scheme for grid tie inverter is proposed. Power expression in synchronous d-q axis will also be given in this chapter.

In chapter 5, the simulation block in Matlab Simulink will be shown in detail based on the model in the last three chapters. Simulation results of the whole micro hydropower system will be given.

# Chapter 2 Micro hydro turbine and permanent magnet synchronous generator

## 2.1 Micro hydro turbine introduction and simplified model

The characteristics of the micro hydro turbine are critical in micro hydropower plant design. It converts the energy from the flowing water to a spinning mechanical energy form which can be used by the generator. In this section, the micro hydro turbine will be quickly reviewed, and detailed mathematical model will be discussed. A simplified turbine expression based on mechanical simulation and experimental results will be shown.

### 2.1.1 Introduction of hydro turbines

There are two main types of hydro turbine: impulse turbines and reaction turbines. Impulse turbines have fixed nozzles which will eject the water and directly shoot it on the turbine moving buckets. The direction of the water will be changed resulting in the turbine spin. The kinetic energy loss in flowing water will partly convert to the mechanical energy of turbine. Typical impulse turbines are Pelton wheels turbines, water wheels and cross flow (Banki) turbine [28]. Reaction turbines extract energy from the fluid by decreasing the pressure, angular momentum, and velocity of the fluid. Fluid pressure changes after flowing out of the rotating nozzle on the rotor. They are more appropriate for low head flow but high flow velocities condition. Typical impulse turbines are Francis turbines and Kaplan turbines.

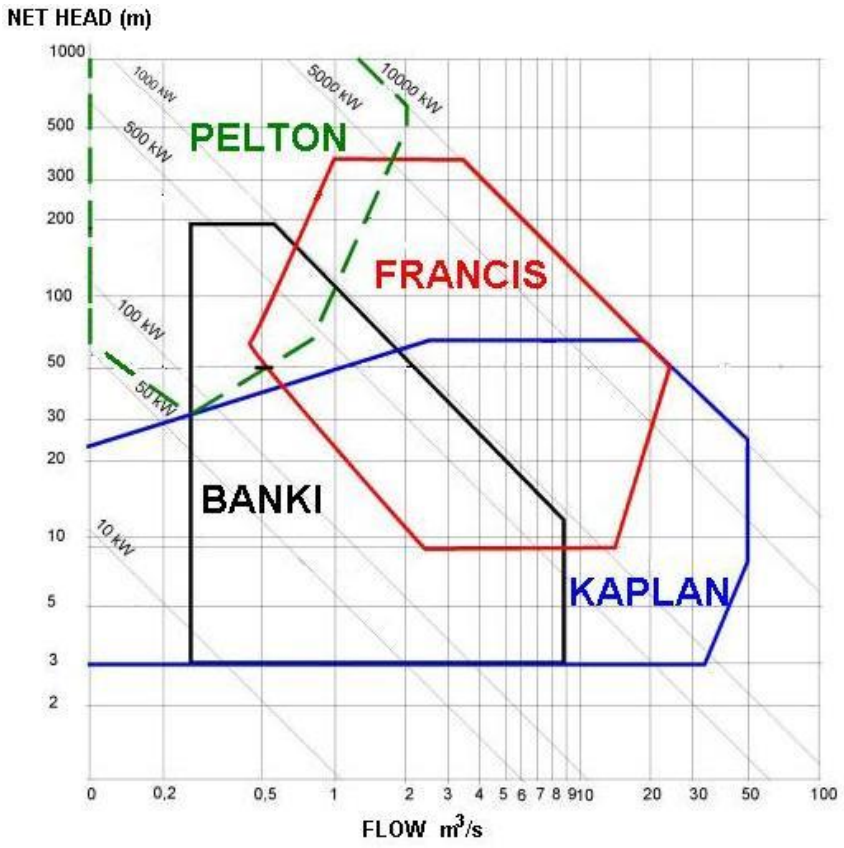


Figure 2-1 Operation range of head and flow for different types of hydro turbine.

The figure 2-1 shows suitable hydro turbine choice under the different head and flows conditions. The Pelton turbine is appropriate for the state that the head is higher than 30m, the flow rate is lower than 2 $m^3/s$ and total power greater than 50 kW. The Francis turbine which occupies the central part of the graph should run at 8~400 m head, 0.5-25 m $m^3/s$ and the power rating of 250 kW and 10 Mw. The Banki turbine working area is under 200m head, 0.3-9 $m^3/s$ flow rate and less than 1Mw. The Kaplan turbine can run at 50 $m^3/s$ flow rate at most with a maximum 70m head and 10Mw power.

For traditional hydro plants, Pelton and Francis will be a good choice because of their large power and head capacities. However, for a micro hydro power plant which means the rating power is less than 100Kw, the Kaplan turbine has the largest operation area

compared to others. It is also the only turbine that can work below 10Kw power rating. Based on these considerations, Kaplan turbine is the best choice of our micro-hydropower turbine for power generation. The detailed modeling of the turbine will be introduced in next section.

### 2.1.2 Modeling of micro hydro turbine

Kaplan turbine is a reaction turbine with propeller (runner blades) and wicket gate which can adjust the water flow. The water flows directly to wicket gate and is perpendicular to the propeller. The water falls through runner blades because of the gravity force and cause the turbine to spin.

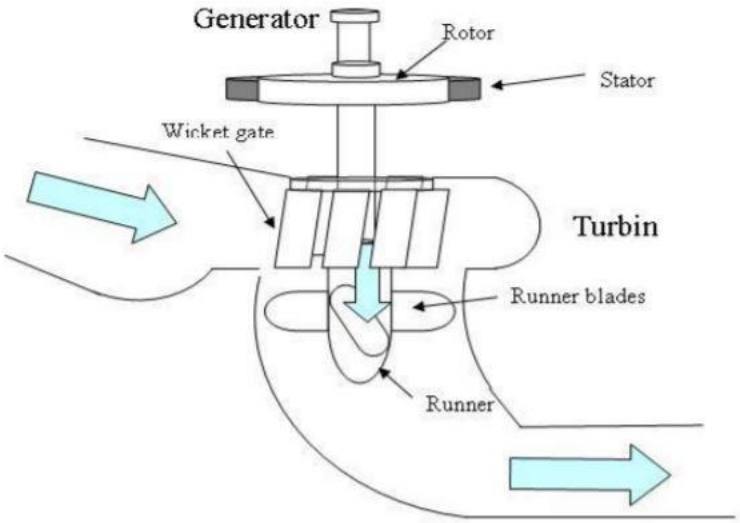


Figure 2-2 Insight view of Kaplan turbine operation principle with a generator [29].

Figure **Error! Reference source not found.** shows an insight view of the Kaplan turbine. A specially designed nozzle is the outlet of water which can decelerate the water speed. The decrement of speed will lower the pressure on the outlet side. Thus, the pressure difference between inlet and outlet will increase which can increase the

water flow through the blades and extract more power from the water. The available output hydropower can be expressed as follows:

$$P_{hydro} = \rho * g * H * Q$$

Where ρ is the water density (kg/m$^3$), g is the gravity acceleration (m/s$^2$), H is the head of water (m), and Q is water volume flow rate(1/s).

The turbine efficiency is described as follows:

$$\eta = \frac{P_{turbine}}{P_{hydro}}$$

where:

$$P_{turbine} = T * \omega$$

T is the torque of the turbine and ω is the rotation speed of the turbine. We can see that under a particular water flow condition, the efficiency is proportional to the rotation speed.

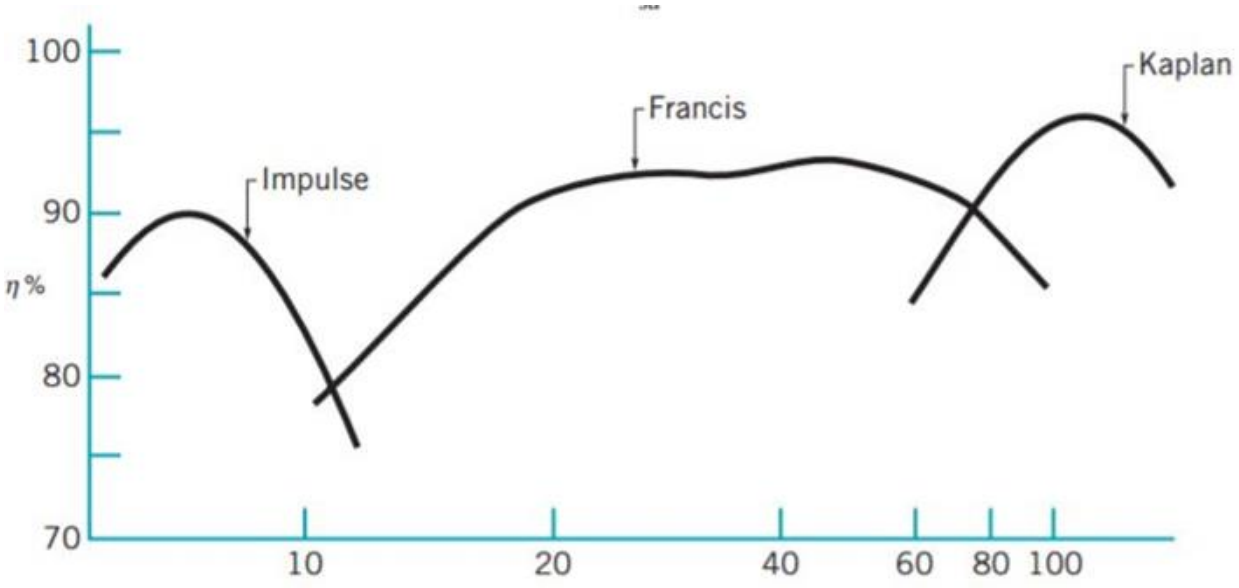


Figure 2-3 Turbine efficiency versus rotation speed for Impulse, Francis, and Kaplan turbine [30].

Figure **Error! Reference source not found.** shows a typical efficiency-speed curve for three different types of hydro turbines. These efficiency characteristic curves have a similar shape: the efficiency will reach at a maximum point under a certain rotation speed of the turbine. However, unlike the well-developed wind turbine which has a specific tip speed ratio for the maximum efficiency, the hydro turbine does not have a general expression of efficiency and speed. The maximum efficiency speed is mainly based on the individual turbine design. In next section, a particular Kaplan turbine simulation and experimental results will be analyzed.

### 2.1.3 A simplified model of the hydro turbine.

A complicated model of Kaplan turbine contains many other modeling like penstock modeling, wicket gate modeling, hydraulics modeling and mechanical modeling[30]. In this thesis, these modelings are eliminated because of the difficulty and complexity. A specific simulation and experimental result from Dr. Ryoichi Amano is used in this research.

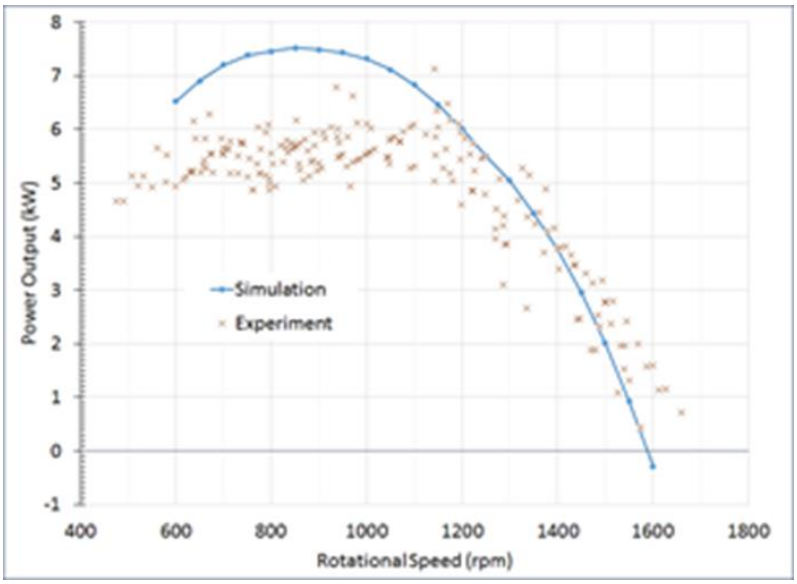


Figure 2-4 Power-speed curve simulation result of a Kaplan turbine under a certain head flow gained from Dr. Ryoichi Amano.

The blue line is the simulation result of the power-speed relationship curve of a Kaplan turbine under a particular head and flow rate. As we can see that the turbine will reach the maximum power and efficiency when the turbine rotates at around 880 RPM. And the shape of the curve is a typical parabola form.

Table 2-1 Turbine simulation result data gained from the speed-power cruve.

| Power (watt) | Speed (RPM) | Speed (rad/s) | Torque (N/m) |
|---|---|---|---|
| 6500.00 | 600.00 | 62.83 | 103.45 |
| 6900.00 | 650.00 | 68.07 | 101.37 |
| 7200.00 | 700.00 | 73.30 | 98.22 |
| 7300.00 | 750.00 | 78.54 | 92.95 |
| 7400.00 | 800.00 | 83.78 | 88.33 |
| 7500.00 | 850.00 | 89.01 | 84.26 |
| 7450.00 | 900.00 | 94.25 | 79.05 |
| 7400.00 | 950.00 | 99.48 | 74.38 |
| 7300.00 | 1000.00 | 104.72 | 69.71 |
| 7050.00 | 1050.00 | 109.96 | 64.12 |
| 6800.00 | 1100.00 | 115.19 | 59.03 |
| 6400.00 | 1150.00 | 120.43 | 53.14 |
| 6000.00 | 1200.00 | 125.66 | 47.75 |

The table 2-1 shows the data point on the simulation results. The experimental data are not used because of its variation. The torque is calculated according to the equation. The curve has a similar shape with the parabola. Thus, the power can be expressed by speed in a quadratic equation. Matlab function "polyfit" was used to find a quadratic expression of power-speed relationship. With the data that I have, the power equation is derived as follows:

$$\mathrm{P} = -1.23\omega^2 + 223.1\omega - 2623.2$$

Applying equation, we can have torque expression:

$$T_m = -1.23\omega + 223.1 - \frac{2623.2}{\omega}$$

To verify the accuracy of these two expressions, turbine power and torque are calculated with different values of speed and compare to the original simulation data. The table below shows the calculated results of power and torque respectively:

Table 2-2 Regenerated result of the output power based on the power expression equation.

| Speed (RPM) | Speed rad/s | Power ( W ) | Calculated Power(W) | Power Errors | Error percent |
|---|---|---|---|---|---|
| 600.00 | 62.83 | 6500.00 | 6538.74 | -38.74 | 0.52% |
| 650.00 | 68.07 | 6900.00 | 6863.86 | 36.14 | 0.48% |
| 700.00 | 73.30 | 7200.00 | 7121.54 | 78.46 | 1.05% |
| 750.00 | 78.54 | 7300.00 | 7311.77 | -11.77 | 0.16% |
| 800.00 | 83.78 | 7400.00 | 7434.57 | -34.57 | 0.46% |
| 850.00 | 89.01 | 7500.00 | 7489.92 | 10.08 | 0.13% |
| 900.00 | 94.25 | 7450.00 | 7477.83 | -27.83 | 0.37% |
| 950.00 | 99.48 | 7400.00 | 7398.30 | 1.70 | 0.02% |
| 1000.00 | 104.72 | 7300.00 | 7251.32 | 48.68 | 0.65% |
| 1050.00 | 109.96 | 7050.00 | 7036.90 | 13.10 | 0.17% |
| 1100.00 | 115.19 | 6800.00 | 6755.05 | 44.95 | 0.60% |
| 1150.00 | 120.43 | 6400.00 | 6405.74 | -5.74 | 0.08% |
| 1200.00 | 125.66 | 6000.00 | 5989.00 | 11.00 | 0.15% |

Table 2-3 Regenerated results of the mechanical torque obtained from the torque expression equation.

| Speed (RPM) | Speed rad/s | Torque (N/m) | calculated torque(N/m) | Torque error | Error percent |
|---|---|---|---|---|---|
| 600.00 | 62.83 | 103.45 | 104.07 | -0.62 | 0.69% |
| 650.00 | 68.07 | 101.37 | 100.84 | 0.53 | 0.59% |
| 700.00 | 73.30 | 98.22 | 97.15 | 1.07 | 1.19% |
| 750.00 | 78.54 | 92.95 | 93.10 | -0.15 | 0.17% |
| 800.00 | 83.78 | 88.33 | 88.74 | -0.41 | 0.46% |
| 850.00 | 89.01 | 84.26 | 84.15 | 0.11 | 0.12% |
| 900.00 | 94.25 | 79.05 | 79.34 | -0.30 | 0.33% |
| 950.00 | 99.48 | 74.38 | 74.37 | 0.02 | 0.02% |
| 1000.00 | 104.72 | 69.71 | 69.25 | 0.46 | 0.51% |
| 1050.00 | 109.96 | 64.12 | 64.00 | 0.12 | 0.13% |
| 1100.00 | 115.19 | 59.03 | 58.64 | 0.39 | 0.43% |
| 1150.00 | 120.43 | 53.14 | 53.19 | -0.05 | 0.06% |
| 1200.00 | 125.66 | 47.75 | 47.66 | 0.09 | 0.10% |

From these two tables, we can see that the calculated errors are relatively small compared to the actual values. Most of the error percentages are less than 1%. Such a simplified quadratic form expression shows a good accuracy to reproduce the turbine characteristic curve. A similar curve was plotted in Matlab for a better comparison with the original result.

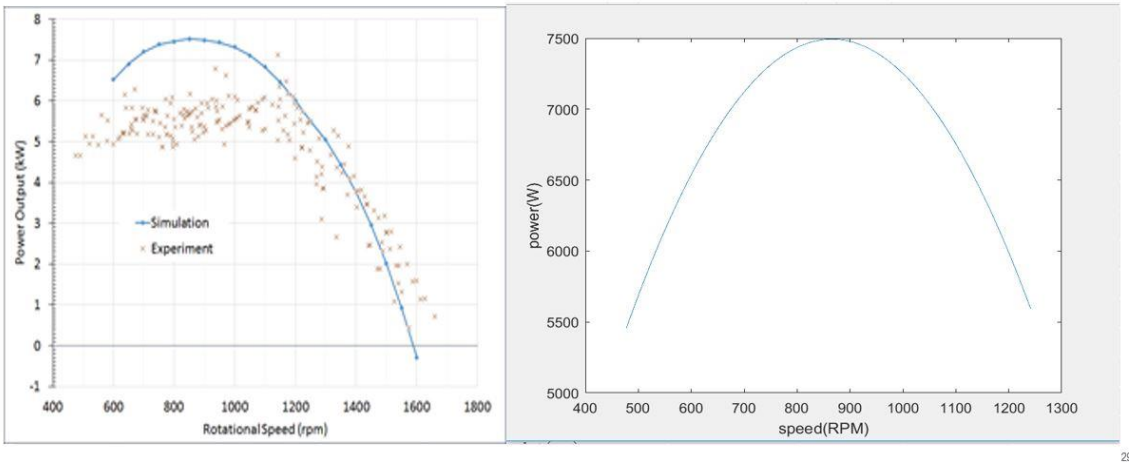


Figure 2-5 Power-speed curve plotted by MATLAB (on the right) compared with the simulation results.

In the rest part of the thesis, the micro hydro turbine power and torque calculation will be based on this expression.

## 2.2 Modeling of permanent magnet synchronous generator

Permanent magnet synchronous generator (PMSG) is a kind of generator which has permanent magnet material to produce magnetic field instead of using electrical field exciting winding. In this section, PMSG will be briefly introduced, and its mathematical model in both stationary frame and synchronous rotation frame will be analysis. Both electrical equivalent circuit and electrical torque analysis will be induced.

### 2.2.1 Introduction of PMSG

The beginning of PMSG can date back to 1930 when the alnico magnet was discovered. The application of PMSG was limited by the undeveloped semiconductors because power converters play a key role in variable frequency and speed generator circuits. People started to pay more attentions to PMSG application with the progress of key technologies like permanent magnet material, control theory and semiconductor component [24].

PMSG is a very efficient electric machine which is widely used in renewable power generation nowadays. Unlike the traditional synchronous generator, the source of the magnet field in PMSG is the permanent magnet material. Such a moveable magnet field can eliminate field exciting wind in the rotor which means less copper loss and mechanical commutator, brushes or slip rings are not needed in PMSG. The absence of these components brings less loss, smaller size and more convenient maintenance for PMSG. Heat up problem will only happen on the stator which is easier to cool down because no current is needed to excite magnet field on the rotor. In the micro hydropower system, PMSG is selected for these following advantages: higher power density, less maintenance is needed, greater controllability with the elimination of mechanical brushes. Before we model the PMSG, the following assumptions are applied:

(1) Magnetic saturation is negligible.

(2) Induced EMF is sinusoidal.

(3) Eddy current and hysteresis losses are negligible.

(4) Damping effect is negligible.

### 2.2.2 Mathematical model of PMSG in natural ABC frame

Figure**Error! Reference source not found.** shows the cross view of the three phase, two poles PMSG. The ABC windings in the stator are $120^0$ electric angle from each other and the magnetomotive force (MMF) $f_a$, $f_b$ and $f_c$ represent the stationary directions. The d axis represents the flux direction of the permanent magnet which is rotating at the speed $\omega_m$. $\theta_r$ stands for the angle between the flux direction (d-axis) and the stationary a-axis [25].

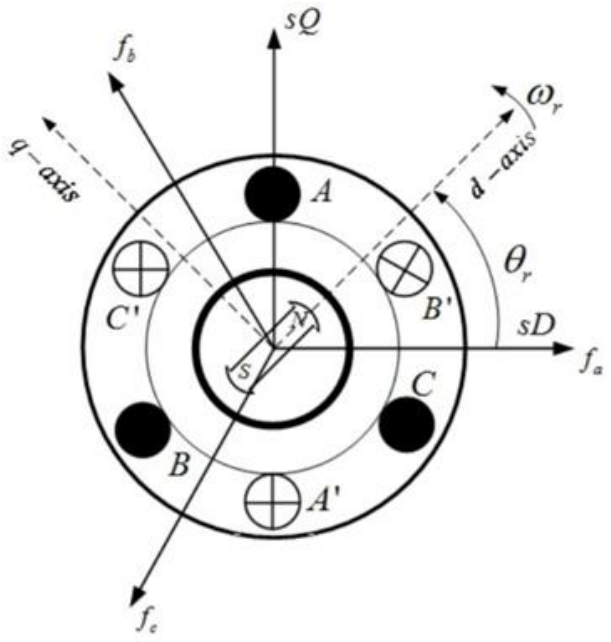


Figure 2-6 Cross view of three phase PMSG with a single pole pair[25].

The stator voltage equations of PMSG in ABC frame regarding phase current and flux linkages can be written as follows [26]:

$$\begin{bmatrix} Va \\ Vb \\ Vc \end{bmatrix} = \begin{bmatrix} Rs\ 0\ 0 \\ 0\ Rs\ 0 \\ 0\ 0\ Rs \end{bmatrix} * \begin{bmatrix} ia \\ ib \\ ic \end{bmatrix} + \frac{d}{dx} \begin{bmatrix} \lambda a \\ \lambda b \\ \lambda c \end{bmatrix}$$

$V_a$, $V_b$ and $V_c$ are stator instantaneous voltages in ABC phase and $i_a$, $i_b$ and $i_c$ are stator instantaneous currents in ABC phase. $R_s$ is the stator winding resistance in ABC phase. $\lambda_a$,$\lambda_b$ and $\lambda_c$ are flux linkages induced by the AC currents and the permanent magnet. The detail expression can be expanded as follows [26]:

$$\begin{bmatrix} \lambda a \\ \lambda b \\ \lambda c \end{bmatrix} = \begin{bmatrix} Laa\ Lab\ Lac \\ Lba\ Lbb\ Lbc \\ Lca\ Lcb\ Lcc \end{bmatrix} * \begin{bmatrix} ia \\ ib \\ ic \end{bmatrix} + \lambda_m \begin{bmatrix} \cos(\omega_m) \\ \cos(\omega_m - \frac{2\pi}{3}) \\ \cos(\omega_m + \frac{2\pi}{3}) \end{bmatrix}$$

$L_{aa}$, $L_{aa}$, and $L_{cc}$ are self-inductance of ABC phase and $L_{ab}$ $L_{ac}$ $L_{ba}$ $L_{bc}$ $L_{ca}$ $L_{cb}$ is mutual inductances respectively for ABC phase. $\lambda_m$ is the flux linkage formed by the permanent

magnet material. As we can see from the equation, both self-inductances and mutual inductances are all functions of rotating speed $\omega_m$. Such a varying time characteristic of inductance cause the difficulty in calculation and analysis. Thus, d-q axis modeling is needed and will be induced in next section.

### 2.2.3 Mathematical model of PMSG in rotational d-q frame

R.H. Park first introduces the dq0 Park's transformation to simplify the synchronous machine models. In the stationary ABC frames of PMSG, the main phase quantities like stator voltages, currents, and flux linkages are depended on time. The 3-phase machine will be analyzed by rotational two-axis. Direct-axis (d-axis) is the direction of rotor magnetic flux and quadrature-axis(q-axis) is perpendicular to d-axis. Under this d-q frame, the varying time characteristic of phase quantities can be eliminated. The ABC to dq0 transformation is shown as follows:

$$\begin{bmatrix} Vd \\ Vq \\ V0 \end{bmatrix} = \frac{2}{3} \begin{bmatrix} \cos(\omega_m t) & \cos(\omega_m t - \frac{2\pi}{3}) & \cos(\omega_m t + \frac{2\pi}{3}) \\ -\sin(\omega_m t) & -\sin\left(\omega_m t - \frac{2\pi}{3}\right) & -\sin(\omega_m t + \frac{2\pi}{3}) \\ \frac{1}{2} & \frac{1}{2} & \frac{1}{2} \end{bmatrix} * \begin{bmatrix} Va \\ Vb \\ Vc \end{bmatrix}$$

The inverse transformation:

$$\begin{bmatrix} Va \\ Vb \\ Vc \end{bmatrix} = \begin{bmatrix} \cos(\omega_m t) & -\sin(\omega_m t) & 1 \\ \cos\left(\omega_m t - \frac{2\pi}{3}\right) & -\sin\left(\omega_m t - \frac{2\pi}{3}\right) & 1 \\ \cos\left(\omega_m t + \frac{2\pi}{3}\right) & -\sin\left(\omega_m t + \frac{2\pi}{3}\right) & 1 \end{bmatrix} * \begin{bmatrix} Vd \\ Vq \\ V0 \end{bmatrix}$$

$V_{dq0}$ represents the voltages on the d-q rotational frame. The transformation can also be applied to the stator current and flux linkages for AC synchronous machine. For a

balanced ABC stationary frame condition, $V_a + V_b + V_c = 0$. Thus $V_0 = 0$ after the Park transformation. By combining the ABC frame model and d-q transformations, the PMSG modeling in d-q axis can be expressed as follows:

$$V_d = i_d R + L_d \frac{di_d}{dt} - \omega_e L_q i_q$$

$$V_q = i_q R + L_q \frac{di_q}{dt} + \omega_e L_q i_q + + \omega_e \lambda_m$$

$$V_0 = i_0 R + L_0 \frac{di_0}{dt}$$

$V_d$,$V_q$, $I_d$, $I_q$, $L_d$, $L_q$ represent the voltage, current, and inductance respectively in the rotational d-q axis. $\lambda_m$ is the flux linkage produced by the permanent magnet material. $\omega_e$ is the electrical rotation speed of the PMSG.From these equations, the equivalent circuit in the d-q frame can be derived:

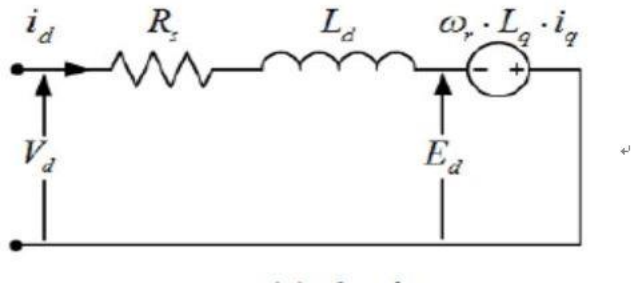


Figure 2-7 Equivalence circuit of PMSG in d-axis.

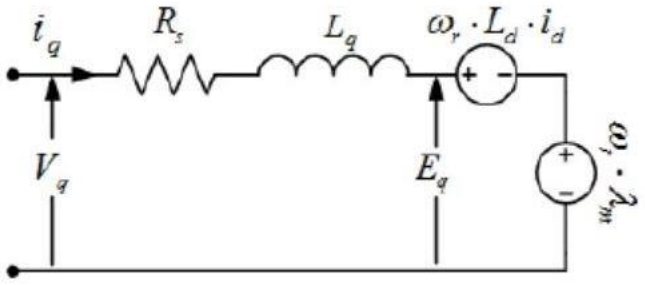


Figure 2-8 Equivalence circuit of PMSG in q-axis.

$L_d$, $L_q$ are synchronous inductance. They are almost equal in the surface mounted

permanent magnet synchronous generators:

$$L_d = L_q = \frac{2}{3}L$$

Where L is, the total inductance tested by the serial-parallel connecting of the stator.

The testing circuit is shown in Figure 2-9[27]:

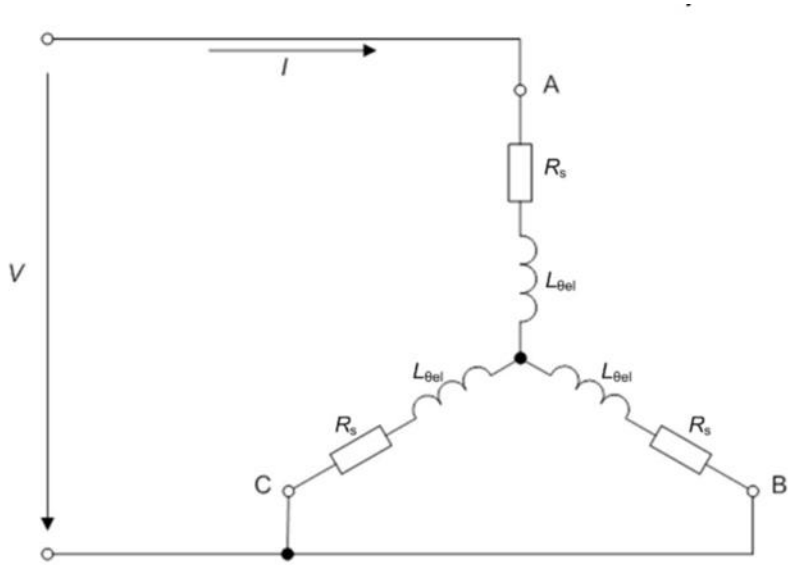


Figure 2-9 Serial-parallel testing circuit for the generator inductance [27].

### 2.2.4Electrical torque and power analysis

Ed and Eq are back electromotive force(EMF) in d-q axis respectively and can be written as:

$$E_d = -\omega_e L_q i_q = -\omega_e \lambda_q$$

$$E_q = \omega_e L_q i_q + \omega_e \lambda_m = \omega_e \lambda_d$$

The mechanical power generated by the PMSG expressed by the d-q axis voltage and current can be expressed as follows:

$$\mathrm{P} = \frac{2}{3}(E_d i_d + E_q i_q)$$

Combine equation we can get:

$$P_m = \frac{2}{3}(\omega_e \lambda_d i_q - \omega_e \lambda_q i_d)$$

The electromagnetic torque expression is:

$$T_e = \frac{P_m}{\omega_m} = \frac{P_m}{\omega_e}(\frac{p}{2})$$

Where $T_e$ is the electromagnetic torque, $\omega_m$ is the mechanical rotation speed, and p is the total number of poles.

Thus, from the equation the electromagnetic torque expressed by the d-q axis elements can be written as:

$$T_e = \frac{3}{2}(\frac{p}{2})(\lambda_d i_q - \lambda_q i_d)$$

Or:

$$T_e = \frac{3}{2}(\frac{p}{2})(\lambda_m i_q - (L_q - L_d) i_q i_d)$$

Since we have assumed that $L_d$=$L_q$, the torque equation can be further simplified as follows:

$$T_e = \frac{3}{2}(\frac{p}{2})\lambda_m i_q$$

The PMSM block model in Simpower library will be directly used in the thesis. The d-q axis equations will be applied to the existing Simulink block.

# Chapter 3 Three phase full bridge diode rectifier and boost converter control

## 3.1 AC to DC rectifier introduction

Two types of AC-DC topologies are commonly used in micro hydropower system. The first one is active PWM rectifiers and the second one is diode rectifiers. The semiconductor components used in active rectifiers are IGBT and diode which can work as both inverter and full bridge rectifiers by manipulating IGBT switches [31]. Such a topology is frequently used in doubly fed induction generator-based system. Thus, it is not going to be employed in this research because of the generator type in the system.

The second topology which is used in this thesis is diode rectifiers. Unlike the PWM rectifiers, we have no control of the output voltage of the rectifier because diodes are passive semiconductor components which don't have a switch to turn on or off.

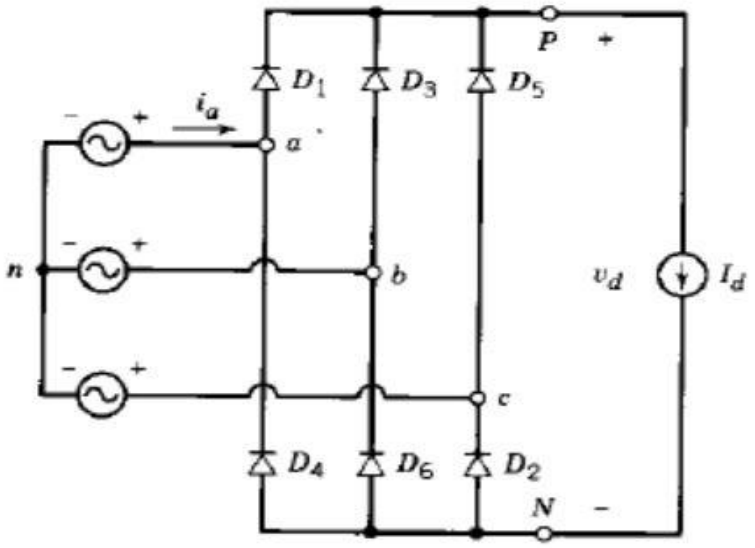


Figure 3-1 Three phase full bridge diode rectifier without line inductance [31].

Figure 3-1 shows a typical three phase full bridge rectifier topology without considering the current commutation effect. Rectifiers are used to converter the AC sine wave voltage with 50 or 60 Hz frequency from utility grid to a DC voltage with ripple. The diode unidirectional conduction characteristic ensures the power will only flow from the AC side to the DC side. This topology will bring massive current distortion of AC side. If the AC source is from the utility, the current distortion problem needs to be considered. However, in this micro hydropower system, the current distortion will not cause as many troubles as it does on the utility grid. Thus, this uncontrolled rectifier is used to be the AC-DC converter because of its unidirectional conducting and simplicity.

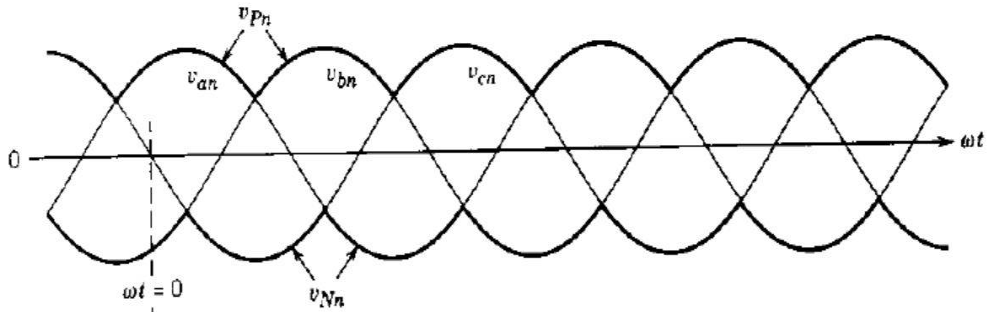


Figure 3-2 Voltage waveform for positive and negative node of the rectifier with a sinusoidal AC input.

The voltage waveform is shown in Figure 3-2.$V_{Pn}$ and $V_{Nn}$ is the voltage at terminal P and N with respect to ground. $V_{an}$, $V_{bn}$, $V_{cn}$ are ABC phase voltage of the AC source. By applying KVL, the instantaneous DC voltage is:

$$V_d = V_{Pn} - V_{Nn} = \sqrt{2}V_{LL}\cos(\omega t)$$

Based on this equation, $V_d$ is plotted as follows:

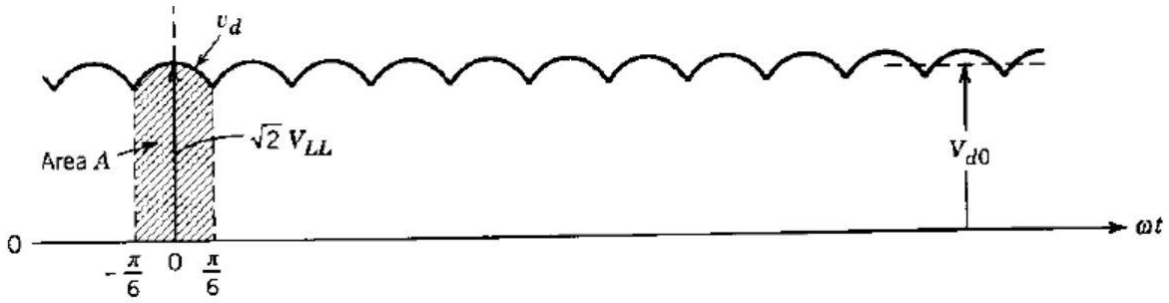


Figure 3-3 Instantaneous rectifier output waveform Vd and voltage-time area A.

From Figure 3-3, we can see that the instantaneous sinusoidal DC voltage can be replaced by an average DC voltage $V_{d0}$ which have the voltage-time area A during the given period. The voltage-time area A can be calculated by the integration of the instantaneous voltage and the expression is given as follows:

$$\mathrm{A} = \int_{\frac{-\pi}{6}}^{\frac{\pi}{6}} \sqrt{2}V_{LL}\cos(\omega t)\, d(\omega t) = \sqrt{2}V_{LL}$$

And the average DC output voltage then equals the area divided by the time which is given as follow:

$$V_{dout} = \frac{A}{\pi/3} = \frac{3\sqrt{2}}{\pi} V_{LL} = 1.35 V_{LL}$$

Where $V_{dout}$ is the average DC output voltage of the rectifier and $V_{LL}$ is the line to line voltage of the AC source. Similar to the voltage RMS analysis we can have the current expression as follows:

$$I_d = \sqrt{\frac{3}{2}} I_s = 1.225 I_s$$

As we can see from both current and voltage expression of the rectifier output, there is no degree of freedom for control for either voltage and current. However, the DC bus needs to be maintained within a certain range for a grid connected topology because of the stability problem. Thus, a boost converter is needed for DC bus voltage control and will be introduced in next section.

## 3.2 Boost converter model

The boost converter is a switched-mode power converter which can produce a DC voltage output larger than the DC voltage input. It is widely used in much clean energy application like electric vehicle battery system, PV system and wind power system. An ideal switch boost converter circuit is shown Figure 3-4 [31]:

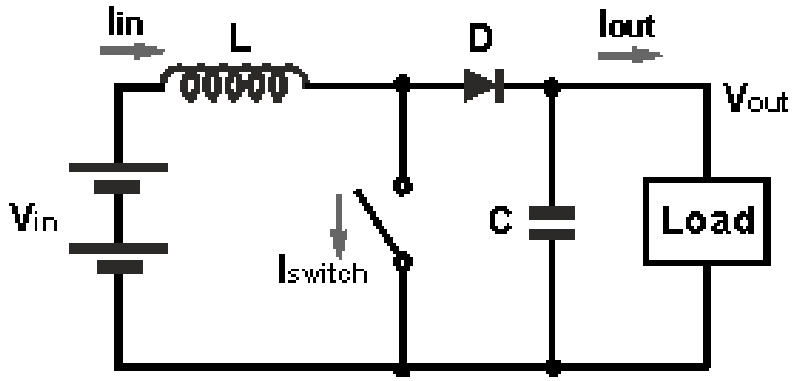


Figure 3-4 Typical DC-DC boost converter topology with ideal switch and diode.

A boost converter usually consists of following components: (1) DC input voltage $V_{in}$, (2) inductor L, (3) semi-conductor switch, (4) diode, (5) output capacitor (6) output load. The input voltage provides the power to the whole circuit. By turning on and off of the switch, the output voltage will be greater than the input voltage because the inductor has to resist current change when the switch is turning on and off and produce a voltage. The circuit of both on and off mode of switch will be introduced in detail

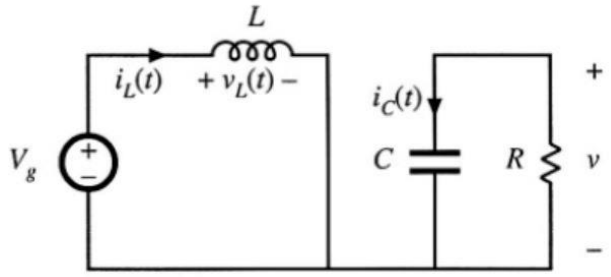


Figure 3-5 Equivalence circuit of boost converter when the ideal switch is on.

When the switch is on, the circuit is shown in Figure 3-5 [32]. The inductor is directly connected to the input voltage, and the capacitor and load resistor are isolated from the input. Ignoring the inductor resistor and capacitor resistor we can have:

$$V_L = V_g$$

$$i_c = -\frac{V}{R}$$

Where Vg is the input voltage, $V_L$ is the inductor voltage, $i_c$ is capacitor current, V is output voltage, and R is load resistor.

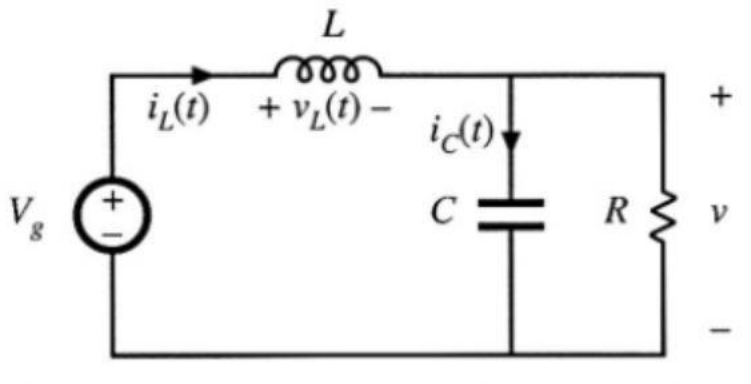


Figure 3-6 equivalence circuit when switch is off

When the switch is off, the circuit is a typical RLC circuit shown in Figure 3-6. The current from in DC input source now can flow to the load side. Now we have a new relationship of the voltage and current in this circuit:

$$V_L = V_g - V$$

$$i_c = I - \frac{V}{R}$$

Where $i_L$ is the inductor current.

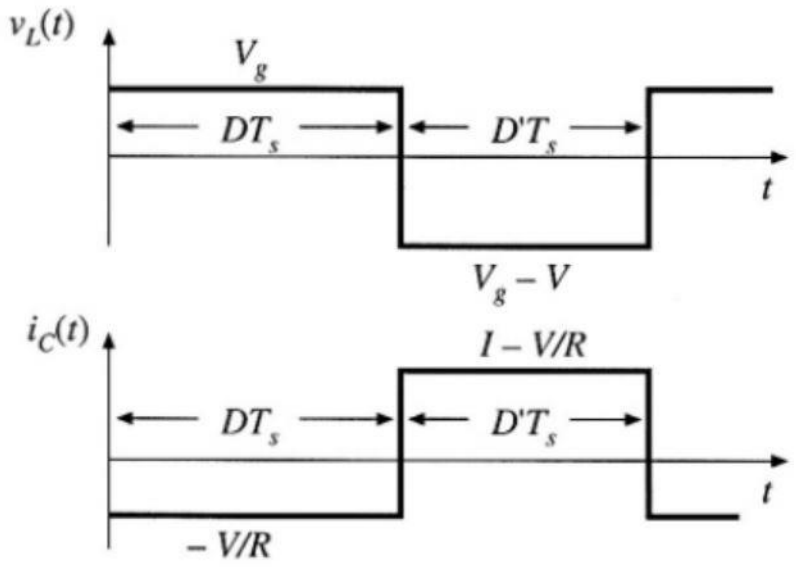


Figure 3-7 Inductor voltage and capacitor current with a single swithcing cycle.

The inductor voltage and capacitor waveform in a single switching period $T_s$ are shown in Figure 3-7. D is the duty cycle which is the portion of on during one cycle and D' is the portion of off in the same cycle. We all know that the inductor and capacitor don't consume energy during a complete switching cycle. Thus, the voltage-second applied on the inductor and current-second applied on the capacitor in each cycle must be zero. Now we have:

$$V_g D T_s + (V_g - V) D' T_s = 0$$

$$-\frac{V}{R} D T_s + \left(I - \frac{V}{R}\right) D' T_s = 0$$

The output voltage and current can be expressed as:

$$\mathrm{V} = \frac{V_g}{D'}$$

$$\mathrm{I} = \frac{V}{D'R}$$

Where:

$$D' = 1 - D$$

From the equation, we can see that with a constant dc voltage input, we can amplify the output voltage within a certain range by controlling the switching duty cycle. When the duty cycle is getting closed to 1, the inductor current will go to infinity based on the calculation. The large current will cause nonlinearity because of the practical inductor resistance and semiconductor forward voltage. Power losses will increase, and the output voltage will drop dramatically.

The ripple of the inductor current and capacitor voltage are important characters that need to be analyzed in boost converter circuit.

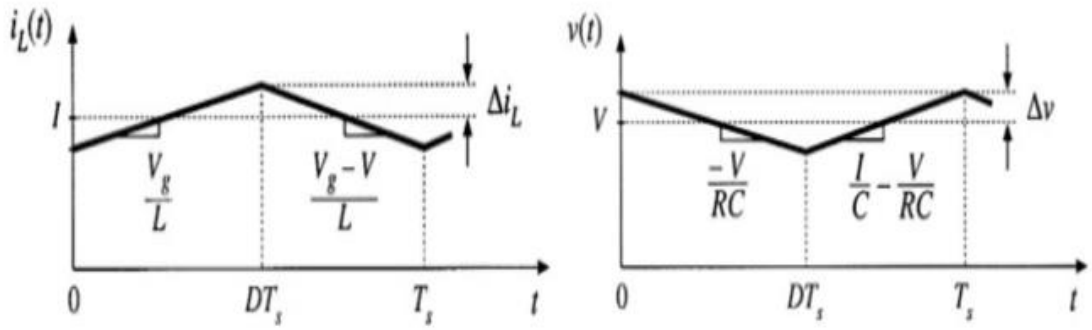


Figure 3-8 Ripple current on the inductor and ripple voltage on the capacitor in one duty cycle.

The inductor current at the on mode is given by:

$$\frac{\mathrm{d}i_L}{\mathrm{dt}} = \frac{V_L}{L} = \frac{V_g}{L}$$

From the current curve, we can see that the total change of current during this period is $2\Delta i_L$. Solve for $\Delta i_L$ we have:

$$\Delta i_L = \frac{V_g}{2L} DT_s$$

The ripple of the inductor current is important because if the ripple current is too large and the calculated negative peak ripple crosses zero, the boost converter must run in

discontinuous conduction mode (DCM). Under the DCM, we can no more apply the equation derived from the continuous conduction mode (CCM). To keep the converter running at CCM, there is a minimum inductance requirement depends on the circuits:

$$L_{min} = \frac{RD(1-D)^2}{2} T_s$$

Like the inductor current, the capacitor voltage at the on mode is:

$$\frac{\mathrm{d}V_c}{\mathrm{dt}} = \frac{i_c}{C} = \frac{V}{RC}$$

The voltage change on the capacitor during the on cycle is $2\Delta V_C$. Solve for $\Delta V_C$ we can derive:

$$\Delta \mathrm{v} = \frac{V}{2RC} DT_s$$

The ripple voltage will directly be applied to the output load. The Large capacitor can eliminate the ripple voltage, but the size and cost will also increase. It is always a tradeoff selection between the capacitor size and maximum ripple voltage on the output.

## 3.3 Boost converter control method

The DC output voltage needs to maintain a constant even with the change of input voltage which also means the generator speed. Thus, feedback control is required in boost converter design. The duty cycle d(t) needs to be manipulated in real-time according to the voltage difference between the output voltage and reference voltage. Usually, the output voltage will be feeding back to the control system, and the transfer function of the control system will be derived. In this thesis, the feedback signal is the inductor current. The output voltage versus duty cycle transfer function V(s)/d(s) is a two-poles form which

will bring difficulty in controller design. However, the inductor current versus duty cycle transfer function i(s)/d(s) is a first order, and such a simple character can bring more degrees of freedom in controller design [33].

### 3.3.1 Small signal analysis of boost converter

The small signal analysis is a dynamic model used to analysis how the perturbation of the input voltage and duty cycle affect the output voltage. From the previous section, we can have the average state equation of inductor and capacitor over a complete switching cycle:

$$\mathrm{L}\frac{\mathrm{d}i_L}{\mathrm{dt}} = V_{in} - D'V_o$$

$$C\frac{\mathrm{d}V_o}{\mathrm{dt}} = D'i_L - \frac{V_o}{R}$$

In this two equation, the input voltage, duty cycle and input current are considered as constants. We also assume that the input current is equal to the inductor current. Right now, small perturbations are added to the state variable signals:

$$i_L = I_L + \widetilde{i_L}$$

$$v_{in} = V_{in} + \widetilde{v_{in}}$$

$$\mathrm{d} = D + \tilde{d}$$

$$v_o = V_o + \widetilde{v_o}$$

$I_L$, $V_{in}$, D, $V_0$ are the quiescent value of the circuit. We also assume that the magnitude of perturbation signals is much smaller than the quiescent value:

$$|\widetilde{i_L}| \ll I_L$$

$$|\widetilde{v_{in}}| \ll V_{in}$$

$$\left|\tilde{d}\right| \ll D$$

$$|\widetilde{v_o}| \ll V_o$$

Plugging the signal with perturbation into the average state equation we can have:

$$\mathrm{L}\frac{\mathrm{d}(I_L + \widetilde{\imath_L})}{\mathrm{dt}} = (V_{in} + \widetilde{v_{in}}) - (D' - \tilde{d})(V_o + \widetilde{v_o})$$

$$C\frac{\mathrm{d}(V_o + \widetilde{v_o})}{\mathrm{dt}} = (D' - \tilde{d})(I_L + \widetilde{\imath_L}) - \frac{V_o + \widetilde{v_o}}{R}$$

Expand this two equation:

$$\mathrm{L}\left(\frac{\mathrm{d}I_L}{\mathrm{dt}} + \frac{d\widetilde{\imath_L}}{dt}\right) = V_{in} - D'V_o + \widetilde{v_{in}} - D'\widetilde{v_o} + V_o\tilde{d} - \widetilde{v_o}\tilde{d}$$

$$\mathrm{C}\left(\frac{\mathrm{d}V_o}{\mathrm{dt}} + \frac{d\widetilde{V_o}}{dt}\right) = D'I_L - \frac{V_o}{R} + D'\widetilde{\imath_L} - I_L\tilde{d} - \frac{\widetilde{v_o}}{R} - \widetilde{\imath_L}\tilde{d}$$

Since the perturbation signal is extremely small compare to the quiescent value, the second order terms which are $\widetilde{v_o}\tilde{d}$ $\widetilde{\imath_L}\tilde{d}$ can be ignored. And from the average state equation, we can know that the quiescent value expression can be canceled by each other. After the cancellation of quiescent value and eliminating the second order perturbation signal we can have:

$$L\frac{d\widetilde{\imath_L}}{dt} = \widetilde{v_{in}} - D'\widetilde{v_o} + V_o\tilde{d}$$

$$C\frac{d\widetilde{V_o}}{dt} = D'\widetilde{\imath_L} - I_L\tilde{d} - \frac{\widetilde{v_o}}{R}$$

These two equations are the state equation with ac perturbation. The figure shows the small signal equivalence circuit based the small signal state equations. In this circuit, we consider the boost converter as a dc transformer with a ratio D':1. The independent current source I$\widetilde{d(t)}$ is riven by the control signal $\tilde{d}$. The transfer function then can be easily derived from the equation and will be discussed in the next section.

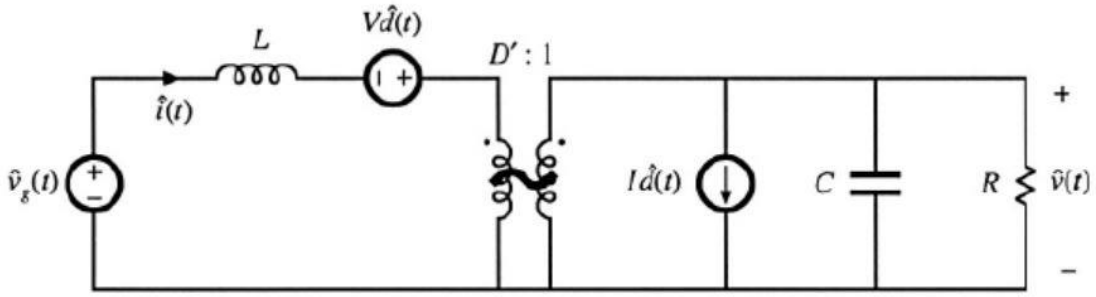


Figure 3-9 Equivalence circuit of a boost converter replaced by a DC transformer with small signal analysis.

### 3.3.2 Transfer function and state space modeling of boost converter

To obtain the transfer function of the boost converter, first we need to take the Laplace transform of the system:

$$sL\widetilde{i_L}(s) = \widetilde{v_{in}}(s) - D'\widetilde{v_o}(s) + V_o\tilde{d}(s)$$

$$sC\widetilde{v_o}(s) = D'\widetilde{i_L}(s) - I_L\tilde{d}(s) - \frac{\widetilde{v_o}}{R}(s)$$

The output voltage, control signal, and inductor current transfer function can be derived from the transfer function.

Duty cycle and output voltage relationship:

$$\frac{\widetilde{v_o}(s)}{\tilde{d}(s)} = \frac{D'V_0 - LI_Ls}{LCs^2 + \frac{L}{R}s + D'^2}$$

Inductor current and output voltage relationship:

$$\frac{\widetilde{v_o}(s)}{\widetilde{i_L}(s)} = \frac{D'V_0 - LI_Ls}{CV_0s + 2D'I_L}$$

Inductor current and output voltage relationship:

$$\frac{\widetilde{i_L}(s)}{\tilde{d}(s)} = \frac{CV_0s + 2D'I_L}{LCs^2 + \frac{L}{R}s + D'^2}$$

From the transfer function, we can see that only the inductor current and output voltage transfer function has first order poles. As mentioned above, this pole characteristic is

more stable than the other characteristic equations which are possible to have a pole on the right half plane. A stable and robust with wide band-with control can be easier to obtain without any other controller. A state space matrix can also be easily derived from the transfer function:

$$\begin{bmatrix} sL & D' \\ D' & -(sC + \frac{1}{R}) \end{bmatrix} \begin{bmatrix} \widetilde{i_L}(s) \\ \widetilde{v_o}(s) \end{bmatrix} = \begin{bmatrix} V_o \\ i_L \end{bmatrix} \tilde{d}(s) + \begin{bmatrix} 1 \\ 0 \end{bmatrix} V_{in}$$

The current control topology for speed control of the generator is shown in Figure 3-10

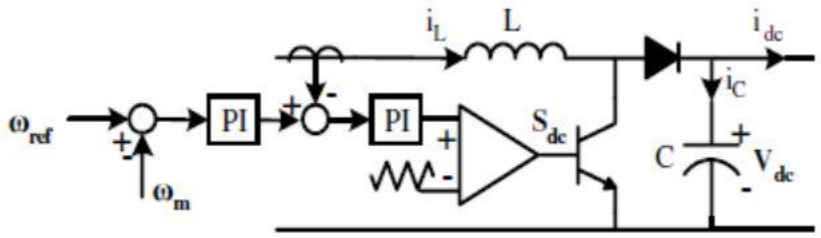


Figure 3-10 Speed control topology with current control of boos converter [35].

The input voltage is directly from the passive diode rectifier which will constantly change with the generator speed. The output voltage of the boost converter will maintain the dc input for the grid-tie inverter which will be discussed in next chapter. The ideal reference speed is generated by the observation & perturbation algorithm. The difference between the real speed and the ideal speed will go through a PI controller and then generate the reference inductor current to control the boost. Simulation results will be shown and discussed in the last chapter.

# Chapter 4 Grid-tie inverter and Perturbation & Observation algorithm

## 4.1 Grid tie inverter

Grid tie inverter plays a major role in many grid-connected distributed power generation systems because it is the converter that controls the quality of power delivered to the grid. The synchronization with the utility grid is the main concern of the inverter control design because the grid frequency and voltage need to be regulated. If the inverter output can't meet the local grid connection criteria, the power will not be allowed to deliver. In our topology, the grid-tie inverter is used to regulate the DC bus voltage and converter the active and reactive power from the DC side to the AC grid.

There are two types of inverter: voltage source inverter(VSI) and current source inverter(CSI). The CSI use a DC current source as an input, and it is only usually used to drive high power AC motor [36]. VSI is more commonly used in grid connection applications. The VSI is driven by a DC voltage source and can be further divided into two types: pulse width modulated inverter (PWM), and space vector modulated inverter(SVM). There are several control methods for VSI like voltage oriented control(VOC), virtual flux based control and direct power control. In this thesis, the VSI with PWM will use VOC and discuss in detail in next two sections.

### 4.1.1 Grid connected VSI with VOC scheme

A simple grid connected inverter driven by a DC voltage source $V_{dc}$ with L filter is shown in the figure. Three phase AC voltages source on the grid are series with a low pass filter L, and line resistor R. The power should flow from the DC side to the AC grid as suggested by current arrow direction. The topology is shown in Figure 4-1:

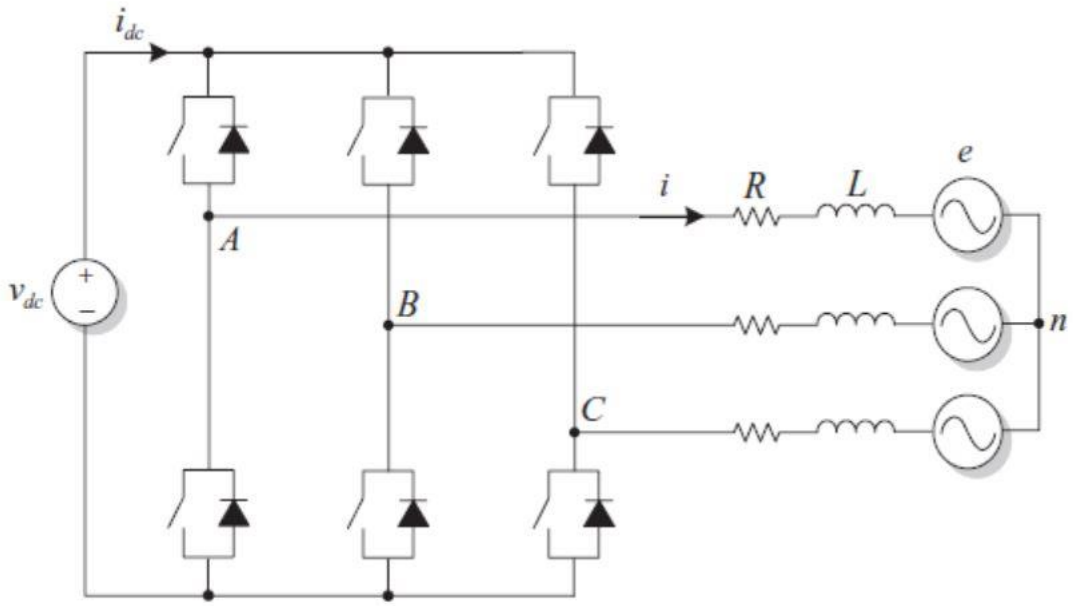


Figure 4-1 Three-phase grid tie inverter model with a grid-side inductor [6].

Before the control is applied to the inverter switches, the mathematical model of L filter inverter needs to be analyzed. The equation describes the inverter output voltage and grid current is:

$$v(t) = e(t) + Ri(t) + L\frac{di(t)}{dt}$$

In this equation, both e(t), v(t) and i(t) are the space vector voltage and current. They are all obtained by the switch function:

$$p(t) = \frac{2}{3}(p_a(t) + \alpha p_b(t) + \alpha^2 p_c(t)$$

Here $p_a(t)$, $p_b(t)$, $p_c(t)$ can only be 0 or 1 depending on the switch state and $\alpha = e^{j2\pi/3}$. All the space vector voltage and current will then be projected to the synchronous frame as we mention in Chapter 2 by the Park transformation. To control the active and reactive power by the inverter, the power expression in the d-q synchronous frame is given as:

$$P_g = \frac{3}{2}(v_{dg}i_{dg} + v_{qg}i_{qg})$$

$$Q_g = \frac{3}{2}(v_{qg} i_{dg} - v_{dg} i_{qg})$$

Where $V_{dg}$ and $V_{qg}$ are grid voltage in d-q synchronous frame and $i_{dg}$ and $i_{qg}$ are grid current in the d-q synchronous frame. If the d-q frame is selected randomly, there will be coupling problem because of the cross product of the d axis component and q axis component. Such a coupling will bring difficulty in inverter control and deteriorate the output power quality and the efficiency. Voltage oriented control (VOC) is induced to solve the coupling problem. Instead of an arbitrary d-q synchronous frame, we can force the d axis to align the phase a space vector and rotate at the synchronous speed. The q-axis voltage will become zero by this synchronization.

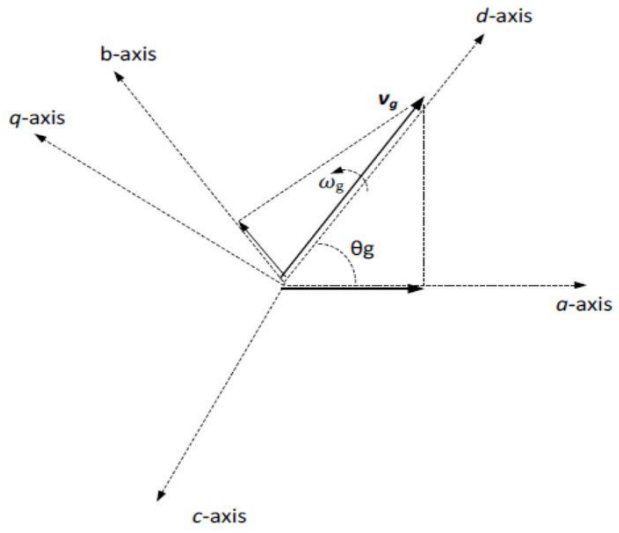


Figure 4-2 Natural ABC frame and rotational d-q frame decomposition with grid frequency $\omega_g$ and a random phase angle $\theta_g$

The synchronous d-q frame diagram in shown in Figure 4-2. Phase a voltage does not have decomposition on q axis because d axis is aligned with it. The decomposition part from phase b and phase c will cancel each other since there are $120^0$ away from each other. Therefore, we have:

$$V_{dg} = V_g$$

$$V_{qg} = 0$$

Put these two value back to power expression in the d-q frame we can have:

$$P_g = \frac{3}{2}(v_{dg} i_{dg})$$

$$Q_g = -\frac{3}{2}(v_{dg} i_{qg})$$

We can see that the q axis current is proportional to the grid reactive power since the grid voltage is a fixed value. A reference is set to control the reactive power sent from the inverter:

$$i_q^* = \frac{Q_g^*}{-1.5 v_{dg}}$$

And if neglect the inverter loss, we have:

$$P_g = \frac{3}{2}\left(v_{dg} i_{dg}\right) = v_{dc} i_{dc}$$

From the equation, neglecting the line resister and reverse the positive direction definition (in VOC modeling, the current flow from the grid to the DC side will be defined as positive) we will have the state-space equation in natural ABC frame:

$$\frac{di_j}{dt} = \frac{e_j - v_j}{L}$$

Where j=a,b,c, and L is the line inductor and considered as the same value in each phase. Transform the state equation into d-q frame we have:

$$\frac{di_{dg}}{dt} = \frac{(e_{dg} - v_{di} + \omega_g L_g i_{qg})}{L_g}$$

$$\frac{di_{qg}}{dt} = \frac{(e_{qg} - v_{qi} - \omega_g L_g i_{dg})}{L_g}$$

After the Park transforms, there is a cross coupling with d axis and q axis current. The PI controller will not be accurate because of the coupling. Thus, we need to subtract the cross-coupling terms and get the following equation for d-q voltage with a PI controller:

$$V_{di} = -\left(k_p + \frac{k_i}{S}\right)\left(i_{dg}^{*} - i_{dg}\right) + \omega_g L_g i_{qg} + e_{dg}$$

$$V_{di} = -\left(k_p + \frac{k_i}{S}\right)\left(i_{qg}^{*} - i_{qg}\right) - \omega_g L_g i_{dg} + e_{qg}$$

Where $K_p$ and $K_i$ are proportional gain and integral gain for PI controller. And the control scheme of VOS for the inverter is shown:

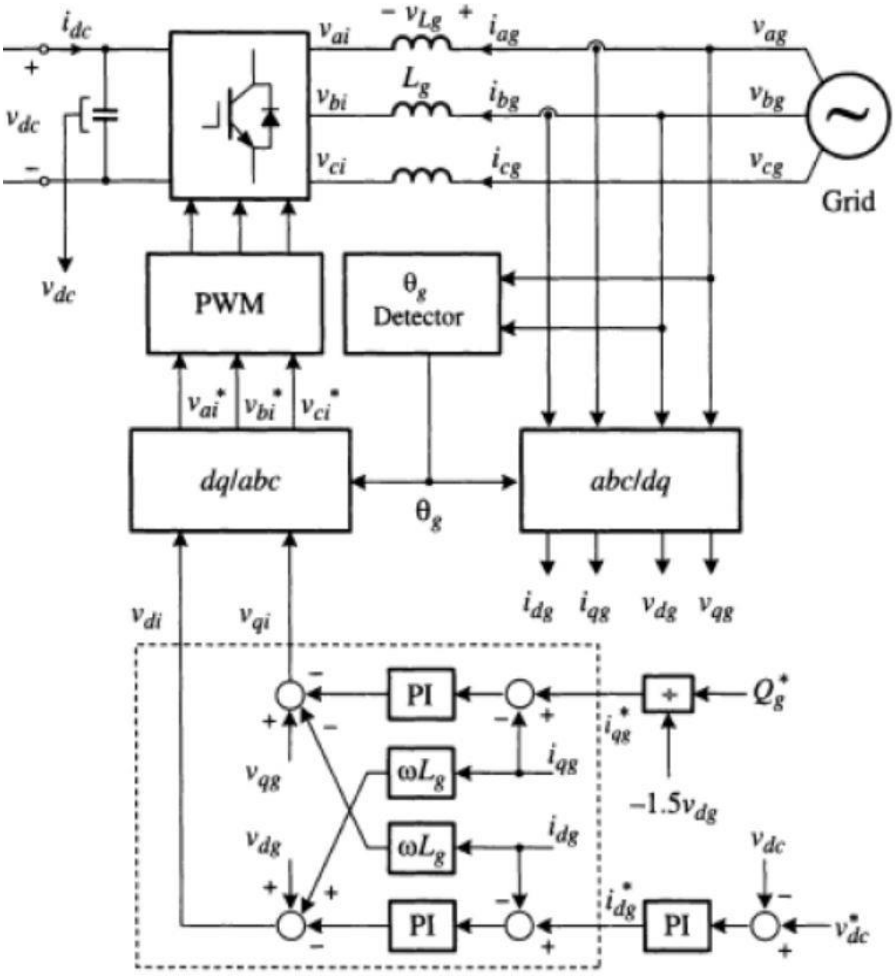


Figure 4-3 Detailed VOC control overview with a grid side converter $L_g$ [6]

### 4.1.2 Phase locked loop for grid synchronization

To synchronize the d-q axis with the natural ABC frame, it is necessary to track the frequency and position of the grid. A phase locked loop system is a closed loop system where an internal oscillator is controlled to keep the time of some external periodical signal by using the feedback loop [37].

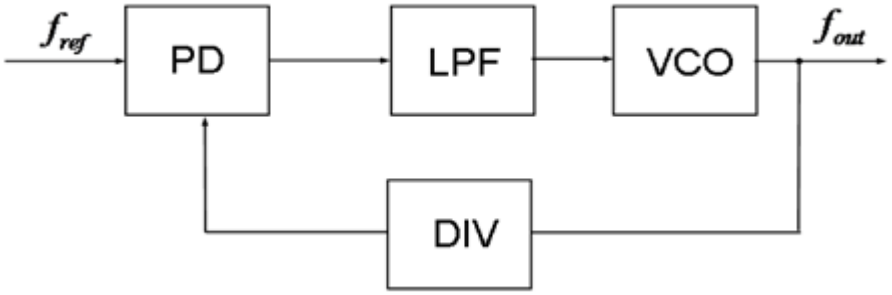


### 4.1.3

Figure 4-4 Detailed PLL block diagram with phase detector low pass filter and voltage controlled oscillator.

A typical PLL diagram is shown in Figure 4-4. It consists of three or four blocks: phase detector (PD), low pass filter (LPF), voltage controlled oscillator (VCO) and an optional output frequency divider(DIV). The PD generate a proportional output signal based on the error between the output frequency and the reference frequency. The output signal is filtered by a low pass filter to avoid mismatch and high-frequency noise and then goes into VCO to generate a signal which has the same frequency as the input signal. By injected the grid voltage signal into the PLL, we can track the phase a voltage frequency and phase angle which is used for Park transformation and synchronize the d-q axis with the natural ABC phase.

### 4.1.4 Sinusoidal pulse width modulation inverter

Generating the right switching signal is critical to the appropriate amplitude and frequency of inverter output voltage. For the sinusoidal pulse width modulation (SPWM)

inverter, the switching gate signal is generated by the comparison of the repeated triangle waveform with the control signal [36]. If the amplitude of control signal is larger than the triangle waveform, the switch will be turned on. Otherwise, the switch will be off. To generate a sinusoidal output voltage with controllable magnitude and frequency, the control signal of PWM is also sinusoidal. There are several devices available for inverter switches: thyristors, bipolar junction transistor (BJT), MOS field effect transistors (MOSFET), gate turns off thyristors (GTO) and insulated gate bipolar transistors (IGBT). The power capacity and switching frequency are listed below for each device:

Table 4-1 Power capacity and switching speed range for different types of switching devices.

| Device | Power capacity | Switching speed |
|---|---|---|
| **Thyristor** | High | Low |
| **BJT** | Medium | Medium |
| **MOSFET** | Low | High |
| **GTO** | High | Low |
| **IGBT** | Medium | Medium |

MOSFET and IGBT are more popular for industrial application because of their high-power gain and conveniences in control. IGBT will be used as inverter switches considering the power rating and switching frequency [40]. Three phase inverter with IGBT topology is shown in Figure 4-5. The parallel diodes provide the path for reactive power control:

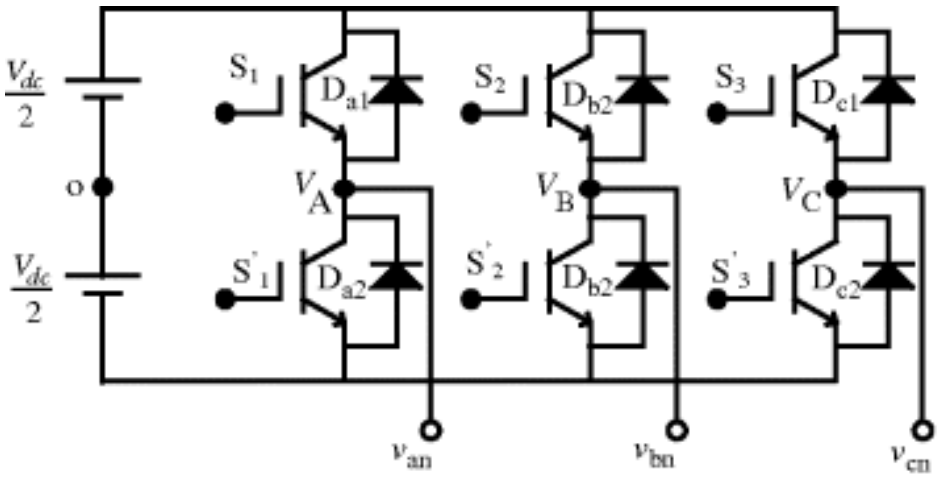


Figure 4-5 Three-phase voltage source inverter topology with IGBT switches and diode.

For each leg of the inverter. The switch is controlled by the following comparison:

$$V_{control-phase\ A} > V_{tri}, T_{A+}\ is\ on$$

$$V_{control-phase\ A} < V_{tri}, T_{A-}\ is\ on$$

$$V_{control-phase\ B} > V_{tri}, T_{B+}\ is\ on$$

$$V_{control-phase\ B} < V_{tri}, T_{B-}\ is\ on$$

$$V_{control-phase\ C} > V_{tri}, T_{C+}\ is\ on$$

$$V_{control-phase\ C} < V_{tri}, T_{C-}\ is\ on$$

The Figure 4-6 shows a typical three phase PWM wave form:

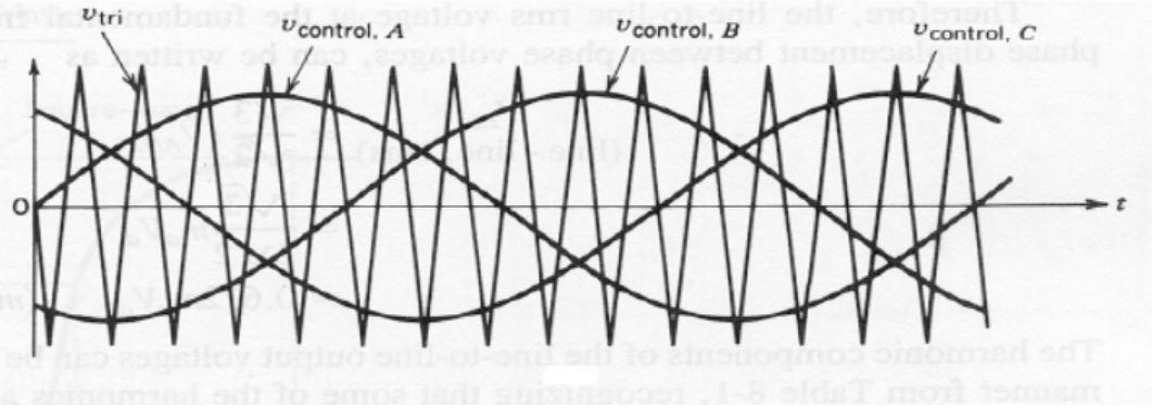


Figure 4-6 Typical PWM triangle waveform with a sinusoidal control waveform [6].

In this PWM, the triangle wave form has a magnitude $v_{tri}$ and frequency $f_s$ (carrier frequency). The sinusoidal control signal has its magnitude $v_{control}$ and frequency $f_1$ (modulating frequency). Since the output voltage is generated by a DC voltage, there are always exist harmonic distortion in the output voltage. The amplitude modulation ratio $m_a$ is given as:

$$m_a = \frac{V_{control}}{Vtri}$$

The frequency modulation ratio $m_f$ is given as:

$$m_f = \frac{f_s}{f_1}$$

Based on the control signal and the comparison algorithm, we can get the output voltage wave form of the leg a, b and phase voltage $V_{ab}$:

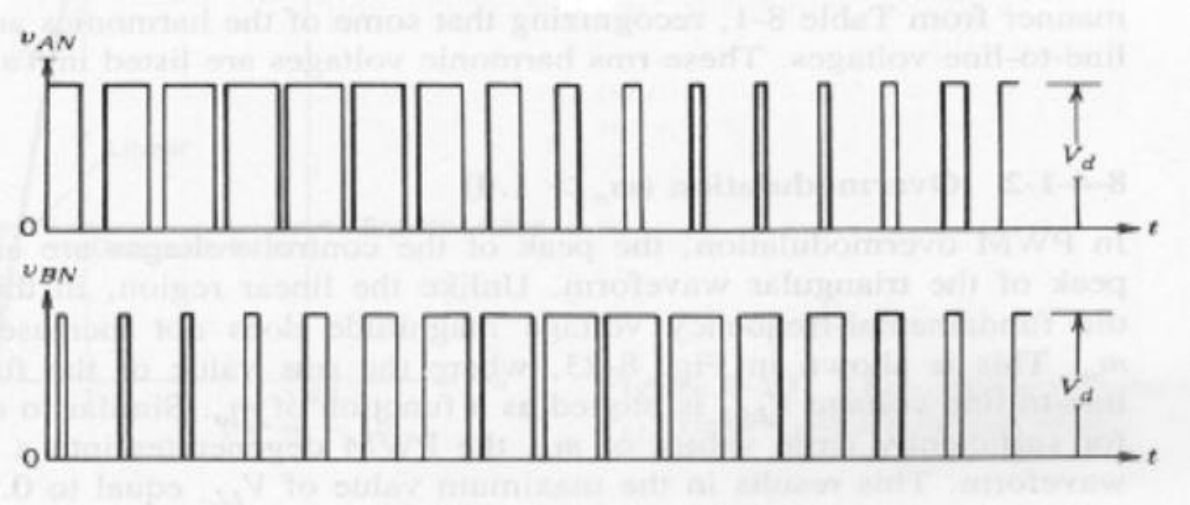


Figure 4-7 Voltage output for leg A and B corresponding to the sinusoidal control waveform [36].

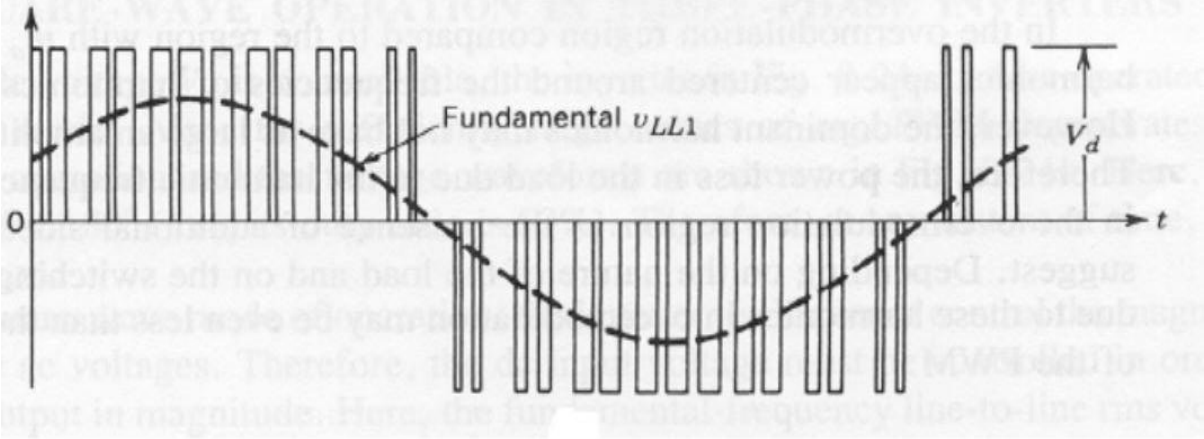


Figure 4-8 Line to line voltage and the fundamental waveform based on the voltage of leg A and B[36].

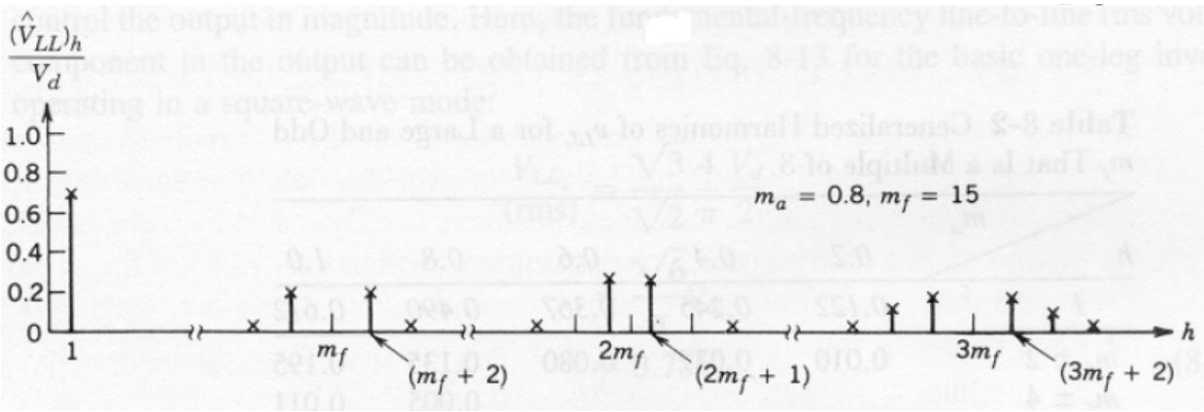


Figure 4-9 Harmonic spectrum of fundamental frequency and high order frequency [36].

Where:

$$V_{AN} = \frac{V_{control}}{V_{tri}} \sin(\omega t) \frac{V_d}{2} = m_a \sin(\omega t) \frac{V_d}{2}$$

$$V_{LL1} = \frac{\sqrt{3}}{\sqrt{2}} V_{AN} = \frac{\sqrt{3}}{\sqrt{2}} m_a \sin(\omega t) \frac{V_d}{2}$$

$$\widetilde{V_{LL1,rms}} = 0.612 m_a V_d$$

$V_{AN}$ is the voltage expression in the time domain, $V_{LL1}$ is the line to line voltage in the time domain. $V_{LL1,rms}$ is the RMS value in the frequency domain. From the harmonic spectrum of the line to lin voltage, we can see that only the harmonics only happen at the odd cycle of $m_f$. Generalized harmonics magnitude of $V_{LL}$ are shown in Figure 4-10:

| $m_a$ / $h$ | 0.2 | 0.4 | 0.6 | 0.8 | 1.0 |
|---|---|---|---|---|---|
| 1 | 0.122 | 0.245 | 0.367 | 0.490 | 0.612 |
| $m_f \pm 2$ | 0.010 | 0.037 | 0.080 | 0.135 | 0.195 |
| $m_f \pm 4$ | | | | 0.005 | 0.011 |
| $2m_f \pm 1$ | 0.116 | 0.200 | 0.227 | 0.192 | 0.111 |
| $2m_f \pm 5$ | | | | 0.008 | 0.020 |
| $3m_f \pm 2$ | 0.027 | 0.085 | 0.124 | 0.108 | 0.038 |
| $3m_f \pm 4$ | | 0.007 | 0.029 | 0.064 | 0.096 |
| $4m_f \pm 1$ | 0.100 | 0.096 | 0.005 | 0.064 | 0.042 |
| $4m_f \pm 5$ | | | 0.021 | 0.051 | 0.073 |
| $4m_f \pm 7$ | | | | 0.010 | 0.030 |

Figure 4-10 Harmonic magnitude look up table for three phase full bridge inverter [36].

## 4.2 Perturbation and Observation algorithm

Perturbation and observation (P&O) algorithm are frequently used in maximum power point tracking in photovoltaic (PV) system because of the easy availability and implementation [39]. The only processing is the measurement of the actual values of PV voltage and current. P&O algorithm can improve the system efficiency regardless of the atmospheric conditions, different kinds of PV panel and panel aging. The output power of the PV panel has a nonlinear relationship with the panel voltage. Figure 4-11shows a typical Power-Voltage characteristic line for the PV panel.

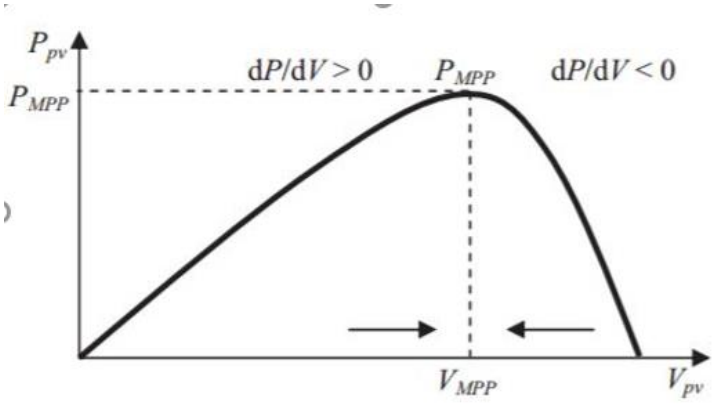


Figure 4-11 Power-voltage characteristic curve for PV with maximum power point[39].

The micro hydropower turbine is experiencing the same situation. The output power is nonlinear with respect to the rotation speed. The speed needs to be adjusted according to different atmospheric conditions. Thus, P&O algorithm is induced to generate the ideal turbine speed irrespective to atmospheric conditions like head flow or turbine setting. The P&O algorithm for the system is given in Figure 4-12:

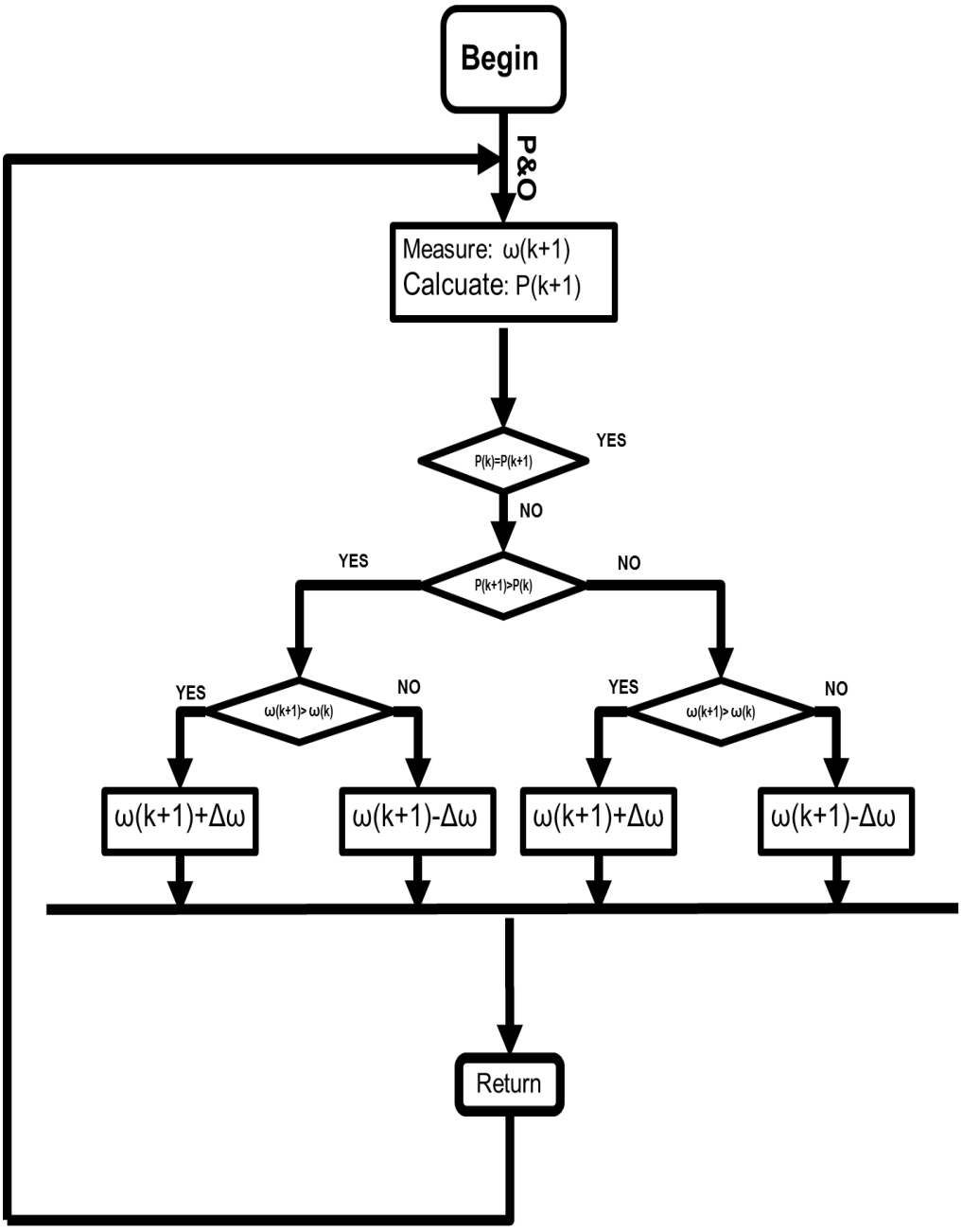


Figure 4-12 Detailed P&O algorithm flow chat for micro hydropower system.

For every certain step time, the turbine power P(k+1) and rotation speed ω(k+1) will be measured and compared with the value in the last step time P(k) and ω(k). By such comparison, the position of the present power point and the direction of the step will be decided. The step size of the algorithm decide the ripple value and response time of the system. For a large step size Δω, it will take less time to reach the maximum power point

(MPP) but larger oscillation at the steady state. A smaller step size Δω will generate less ripple with longer response time. A better way to solve this problem is to increase the frequency of the sampling time and decrease the step size Δω which will give us a fast response and less ripple.

The reference speed generated by the P&O algorithm will then control the boost converter or the grid tie inverter. There are two situation: (1)the reference speed is high enough to produce the DC voltage which can directly fed the grid tie inverter, the duty cycle will directly be set to 0 and work as a bypass circuit and the reference speed will directly control the DC bus voltage by the inverter; (2) the reference is not high enough and need to boost converter to boost up the DC voltage, the reference will control the boost converter duty cycle to maintain the turbine speed at the ideal value

# Chapter 5 Simulation result of the micro hydropower system with conclusion and future work

In this chapter, the whole block diagram will be given and each block of the system will be explained in Matlab Simulink. The output power and speed relationship will be discussed.

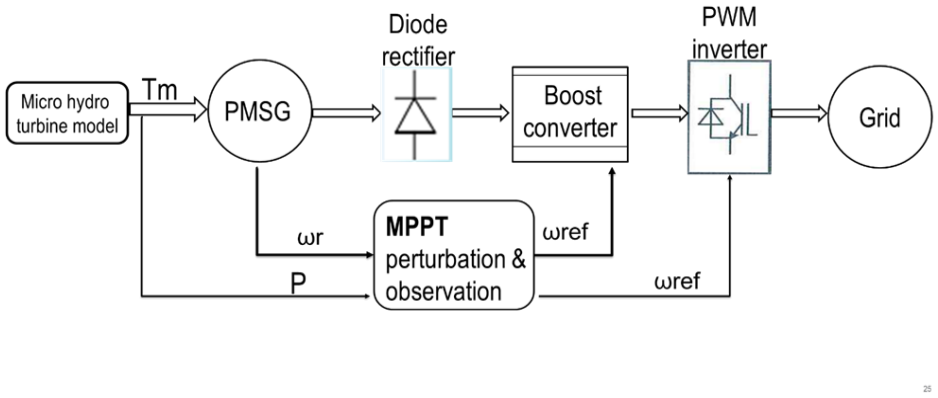


Figure 5-1 Overview block diagram of the micro hydropower system.

figureFigure 5-1 shows the over view of the micro hydro system: the approximated micro hydro turbine will generate a torque with respect to the present generator speed and the produced torque will drive the generator to produce electric power. The P&O algorithm will generate the reference for boost control logic and grid tie inverter control logic. The boost converter will adjust the duty cycle to reach the reference speed and the inverter will maintain the DC bus voltage based on the ideal speed.

### 5.1.1 Detail block diagram drawn in Simulink

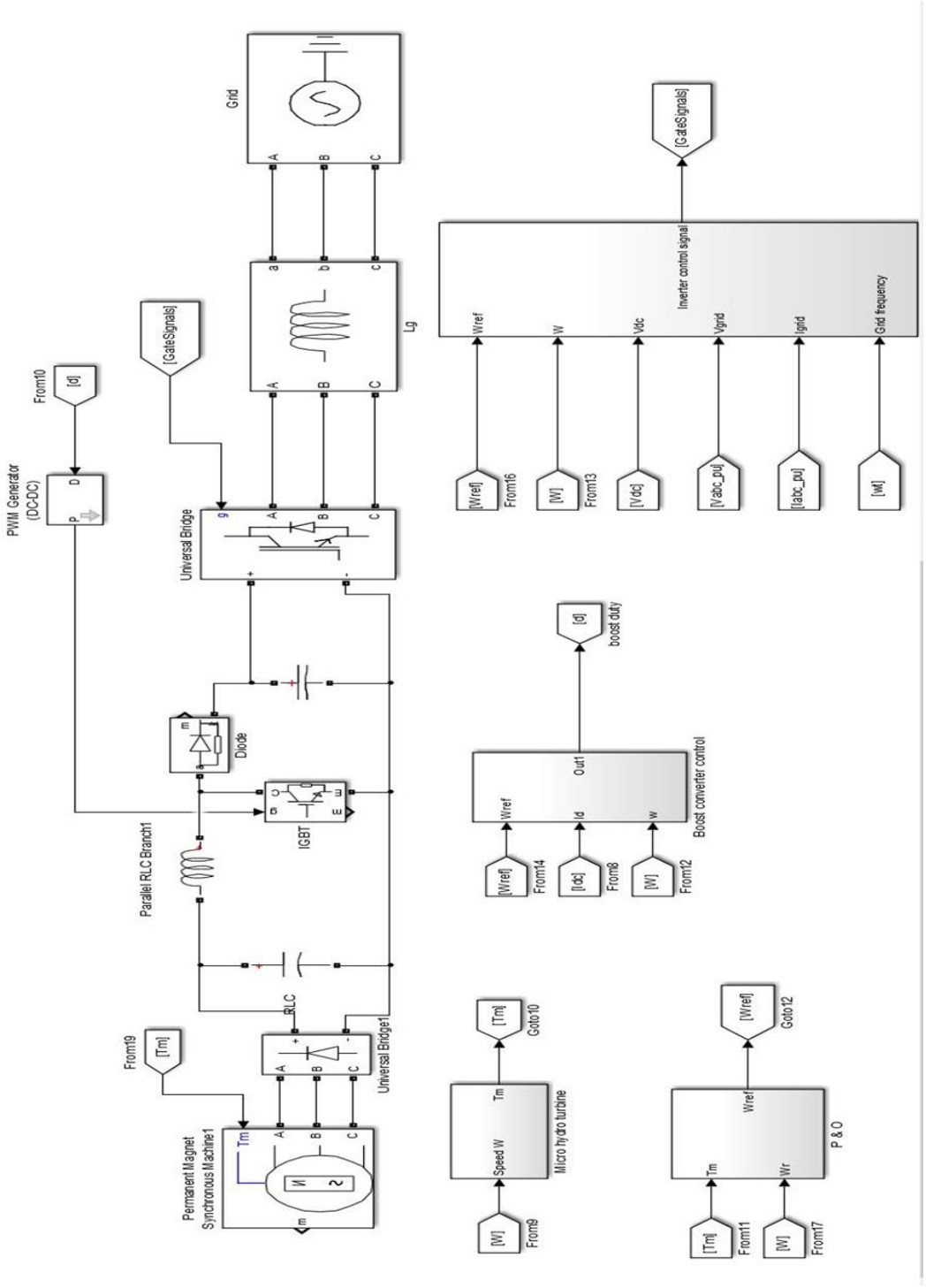


Figure 5-2 Overview block diagram implemented in Simulink.

The system overview in Matlab Simulink is shown in figureFigure 5-2. The detail expression of each model and control block will be given step by step.

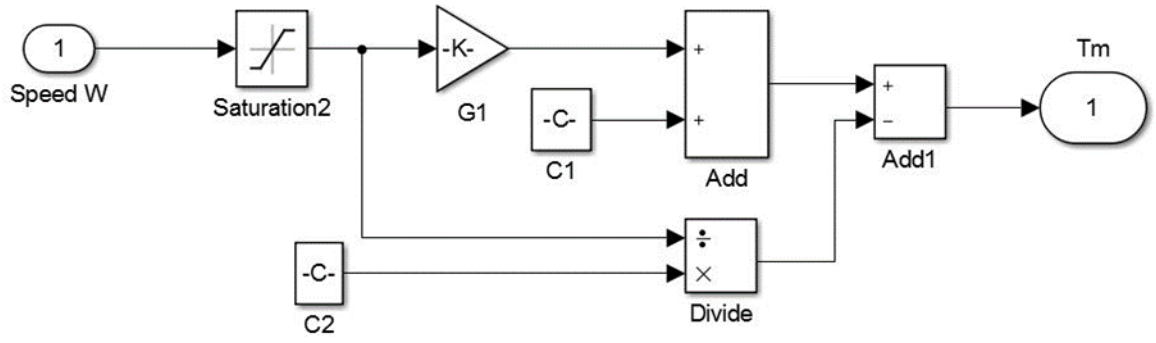


Figure 5-3 Block diagram of the micro hydro turbine torque expression.

The simplified model of the micro hydro turbine is shown in figureFigure 5-3. The turbine model equation is given in chapter 2. The saturation block ensures the turbine speed is in the simulation range which is 480 rpm to 1200 rpm. The torque output will be the input of the PMSG. The torque and power is shown in figure as the speed increases from 480 rpm to 1240 rpm in 8 seconds

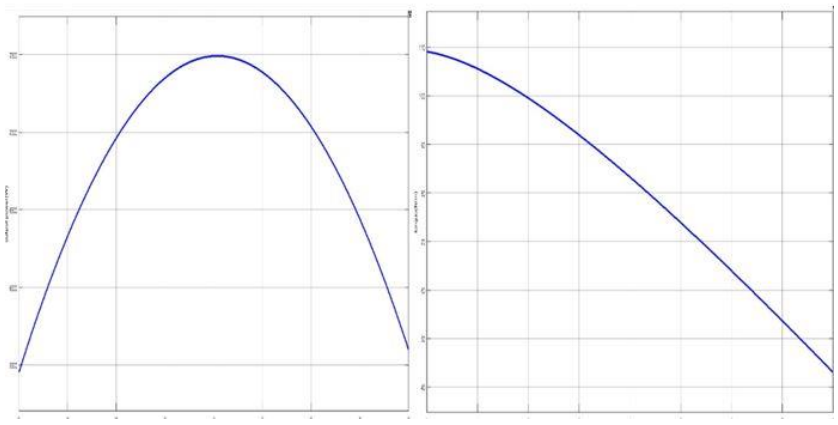

Figure 5-4 Power and torque output versus turbine speed vary from 50 rad/s to 125 rad/s.

The PMSM model in Simulink Simpower Systems machine category is directly used. The required block parameter is shown in table:

Table 5-1 Required PMSM parameters in Simulink.

| Name | Value |
|---|---|
| Back EMF wave form | Sinusoidal |
| State phase resistance($R_s$) | 1.5Ω |
| d-axis inductance($L_d$) | 2.3 mH |
| q-axis inductance(Lq) | 2.3 mH |
| Voltage constant | 650 V_peak L-L/krpm |
| Inertia (J) | 0.00562 $Kg.m^2$ |
| Numbers of poles | 36 |

The boost converter parameter is given in table

Table 5-2 Boost converter parameters for each component

| Name | Value |
|---|---|
| Input capacitor ($C_1$) | 500 μF |
| Induatance(L) | 700 μH |
| Output filter capacitor($C_2$) | 500 μF |
| Diode voltage ($V_f$) | 0.7 V |
| Switching frequency($f_s$) | 10 KHz |
| Output voltage($V_{out}$) | 350V |

The input capacitor is used to decrease the voltage ripple of the rectifier output voltage. The boost converter topology is shown in figureFigure 5-5

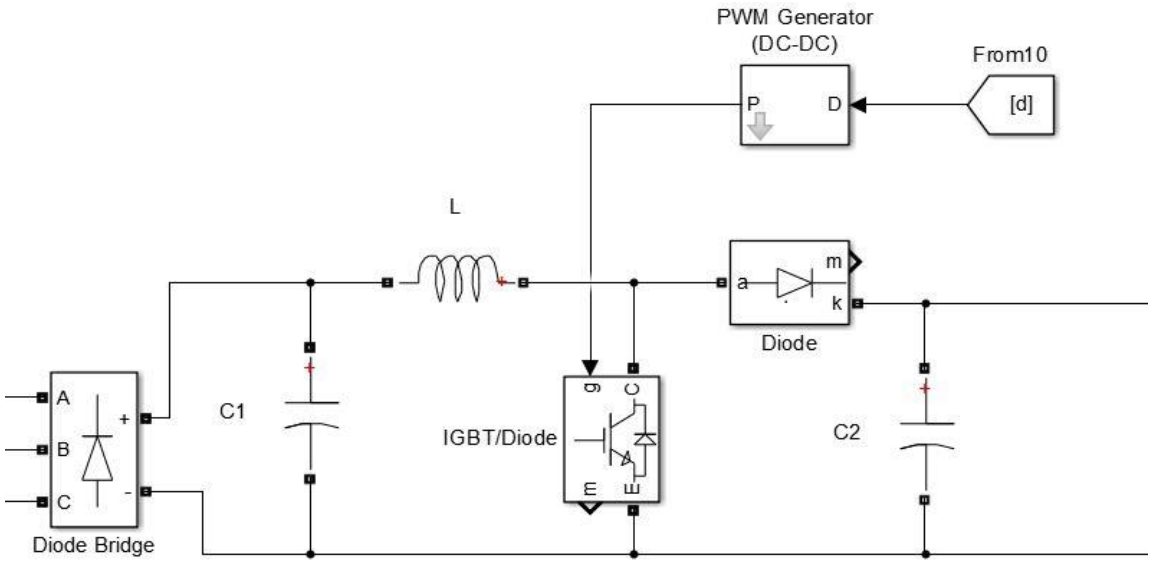


Figure 5-5 Boost converter topology implemented in Simulink.

The current control loop is shown figure Figure 5-6, the error of the speed will go through a PI controller and generate the reference current. The current error will control the duty cycle through another PI controller:

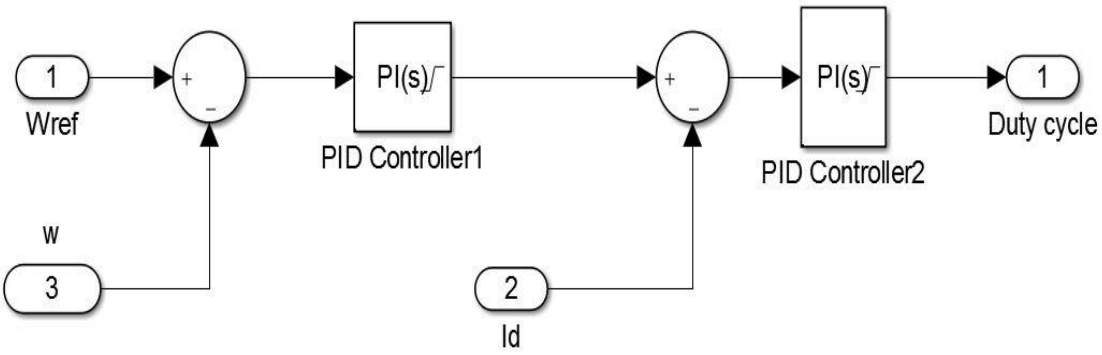


Figure 5-6 Detailed current loop control and speed control loop in Simulink.

The P&O algorithm based on the flow chat is shown in figureFigure 5-7. In this simulation, Δω=0.2 rad/s which is considered as an acceptable step value for both steady state variance and fast response.

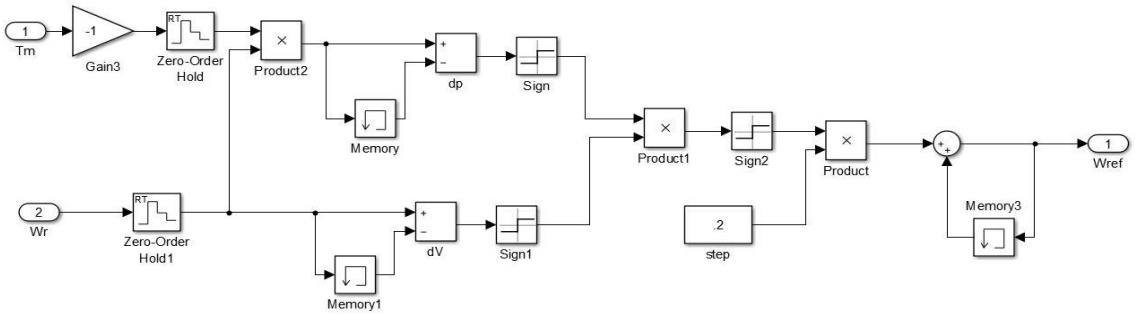


Figure 5-7 P&O algorithm block diagram implemented in Simulink.

The VOC control scheme is shown in figureFigure 5-8 and Figure 5-9, the outside of control can generate the DC bus voltage by comparing the speed difference. d- axis reference current is generated by the DC bus voltage error. The q-axis current is set to be zero. The inner control part is the implementation of the VOC scheme mentioned in chapter 4. The PWM generator is synchronized with the grid frequency with a modulation ratio 34. The Park transformation is provided by the Simulink library.

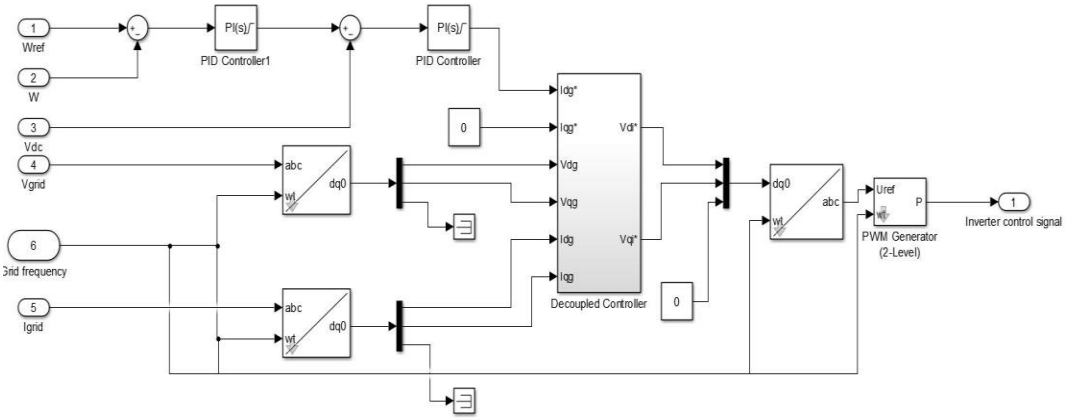


Figure 5-8 Overview grid-tied inverter VOC implemented in Simulink.

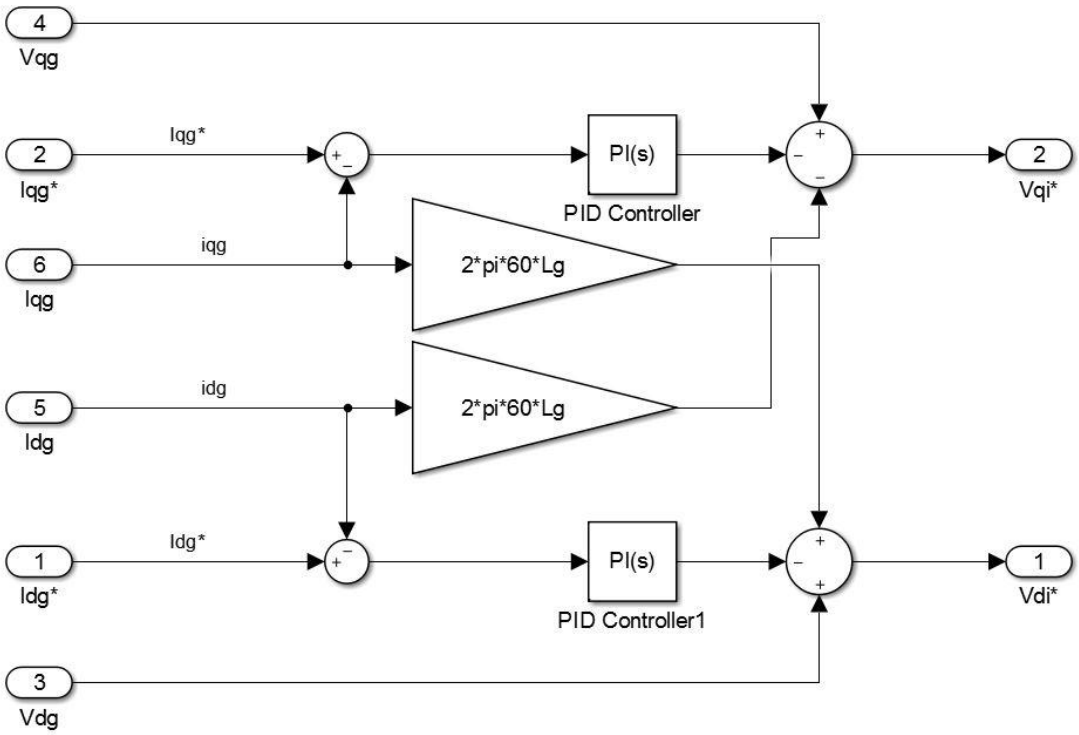


Figure 5-9 Detailed VOC real and reactive power control in Simulink.

The grid angle is generated by the PLL and to synchronize the phase voltage and the d-axis.

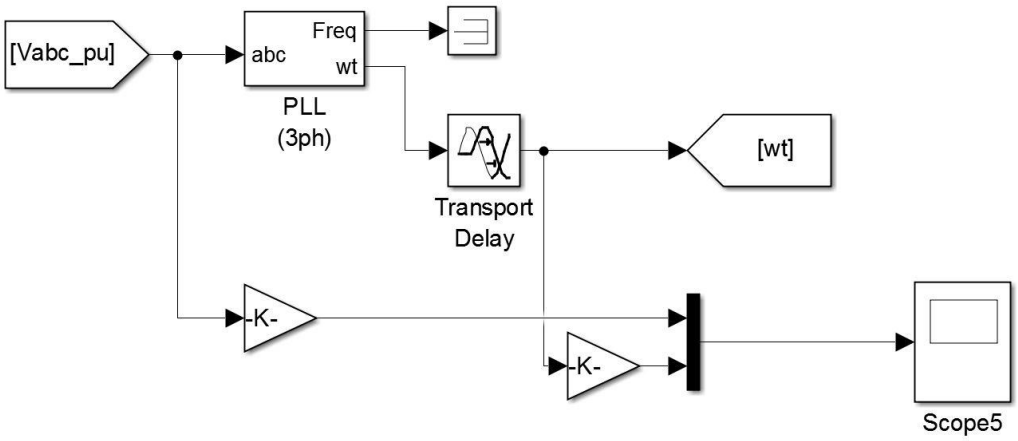


Figure 5-10 Phase lock loop based on the 3-phase PLL block given by the Simulink.

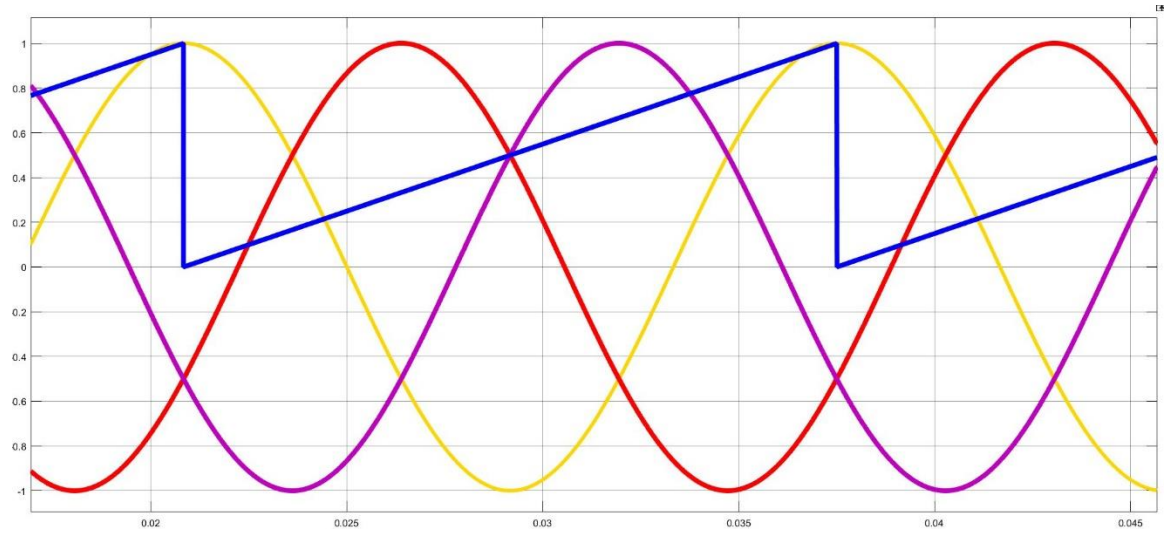

Figure 5-11 Aligned d-axis with the phase a voltage rotating at the same frequency $\omega_t$.

The angle ωt (blue, in P.U.) is aligned with the phase a voltage (yellow, in P.U.). The angle ωt represents the phase a voltage position and will be used for Park transformation and inverter synchronization.

### 5.1.2 Simulation results

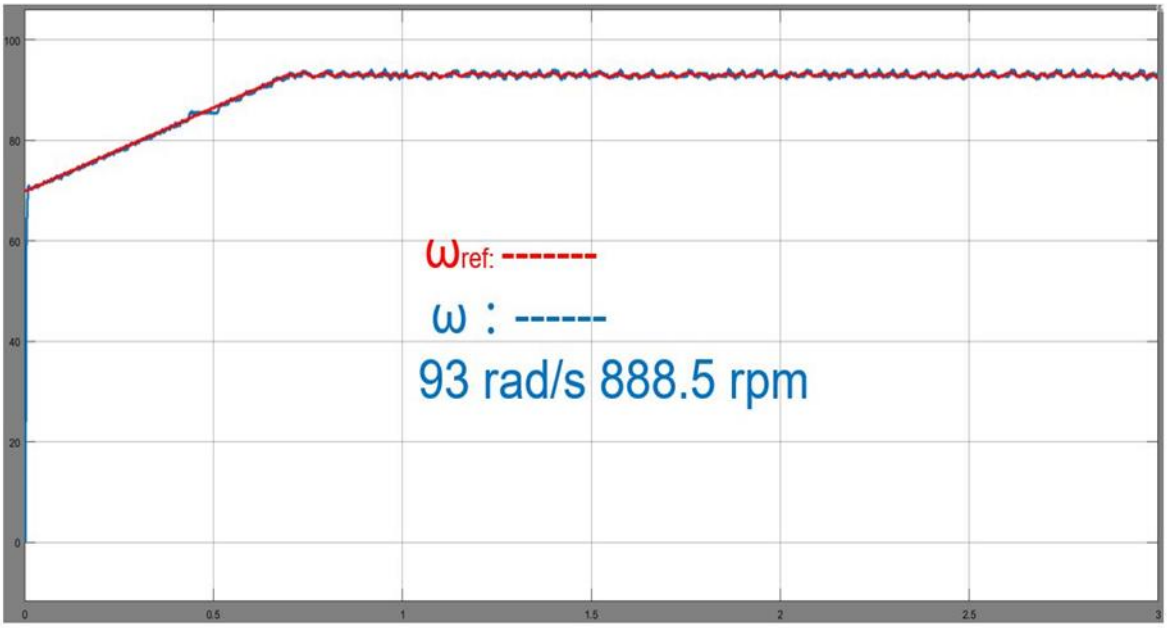


Figure 5-12 PMSG rotation speed and reference speed generated by the P&O algorithm.

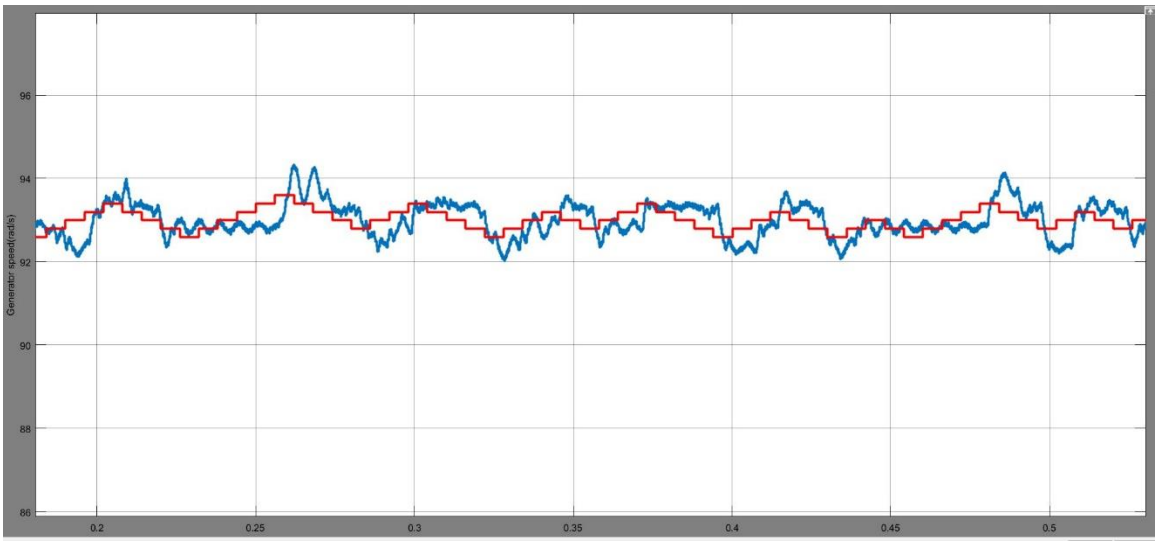


Figure 5-13 Zoom in view of real time speed and the reference speed.

By simulate the whole system, the P&O algorithm will generate an ideal speed and stabilize at 93rad/s (888 rpm) and the boost converter will drive the PSMG rotating at the reference speed shown in figureFigure 5-12. There is steady state oscillation because of the P&O algorithm.

The rectifier output voltage and the boost converter output voltage is shown in figure. When the generator speed is less than 84.4 rad/s, the rectifier voltage is less than 350V which is not high enough to feed the inverter. At this time, the DC bus voltage needs to be boost to 350V. When the generator speed is higher than 84.4 rad/s, the boost converter is not required and the voltage will be controlled by the grid tie inverter and goes higher than 350V.

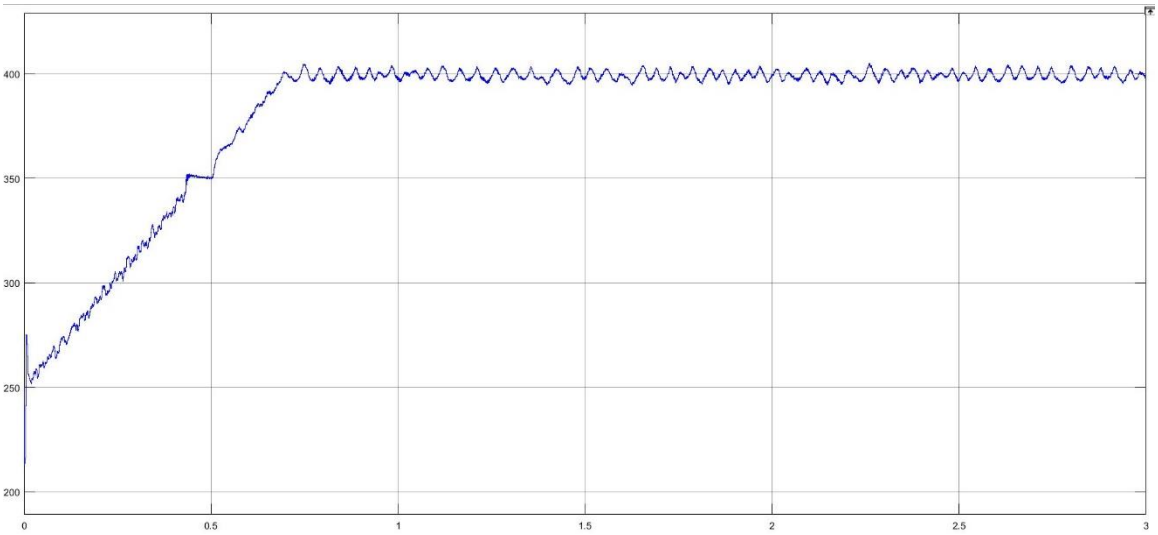


Figure 5-14 Rectifier DC output voltage

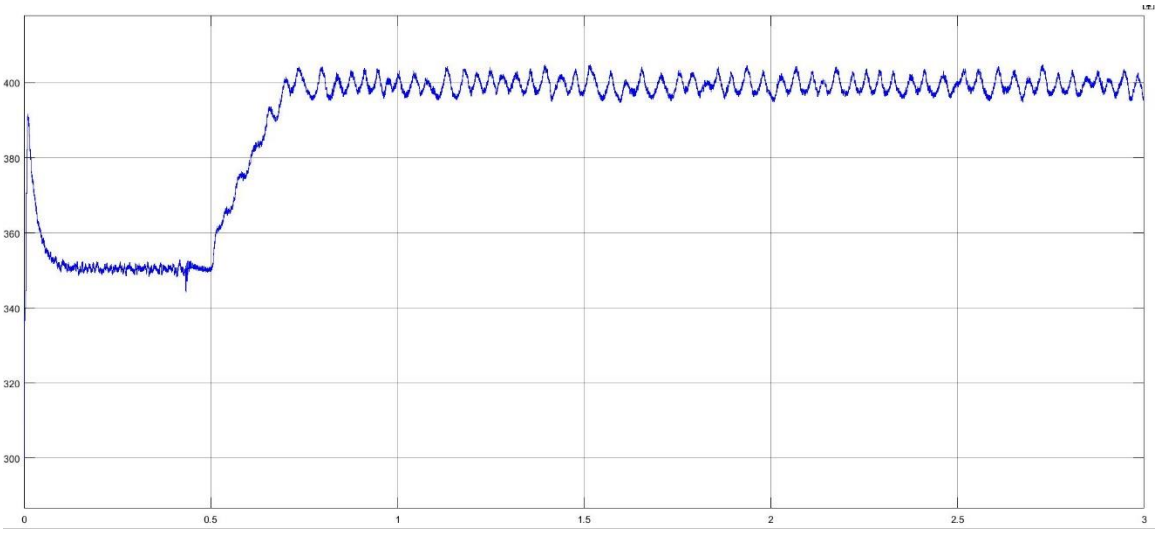


Figure 5-15 Boost converter output voltage and inverter input voltage.

The power delivered to the grid is shown in figureFigure 5-16. The power is increasing as the PMSG speed increases to the ideal speed of the system. Both average value and instantaneous value of the real power is presented. The real power converted to the grid is increasing with the generator speed and reach its maximum value at steady state. The average value is gained from the mean value block of the Simulink. The reactive power

is shown in figureFigure 5-17. As the reference $I_q$ is maintained as zero, the reactive power output is zero.

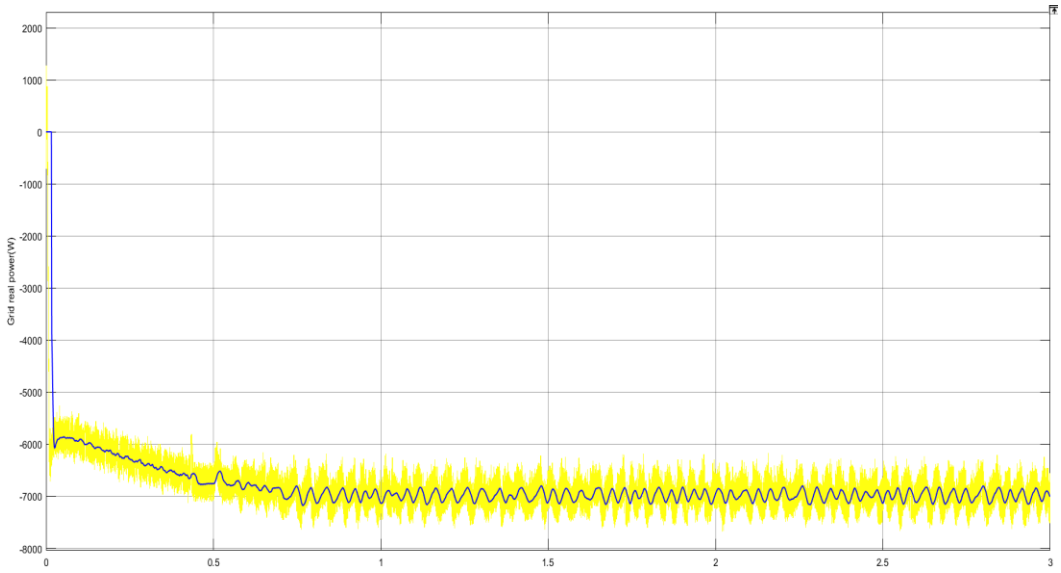


Figure 5-16 Instantaneous and average real power delivered to the Grid.

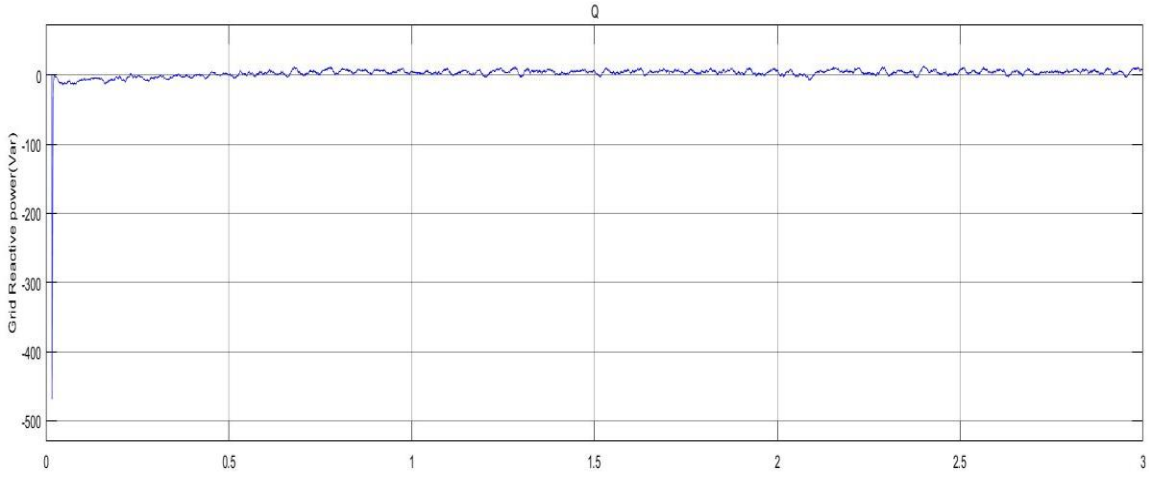


Figure 5-17 Instantaneous reactive power delivered to the Grid

The grid current in d-q axis frame is shown in figureFigure 5-18. The real power is proportional to the d axis current and the reactive power is proportional to the q axis current. As we can see from the figure that $I_d$ has the same tendency with the real power

of the grid. And the q axis current oscillates around zero. The control voltage for each leg is shown in figureFigure 5-19.

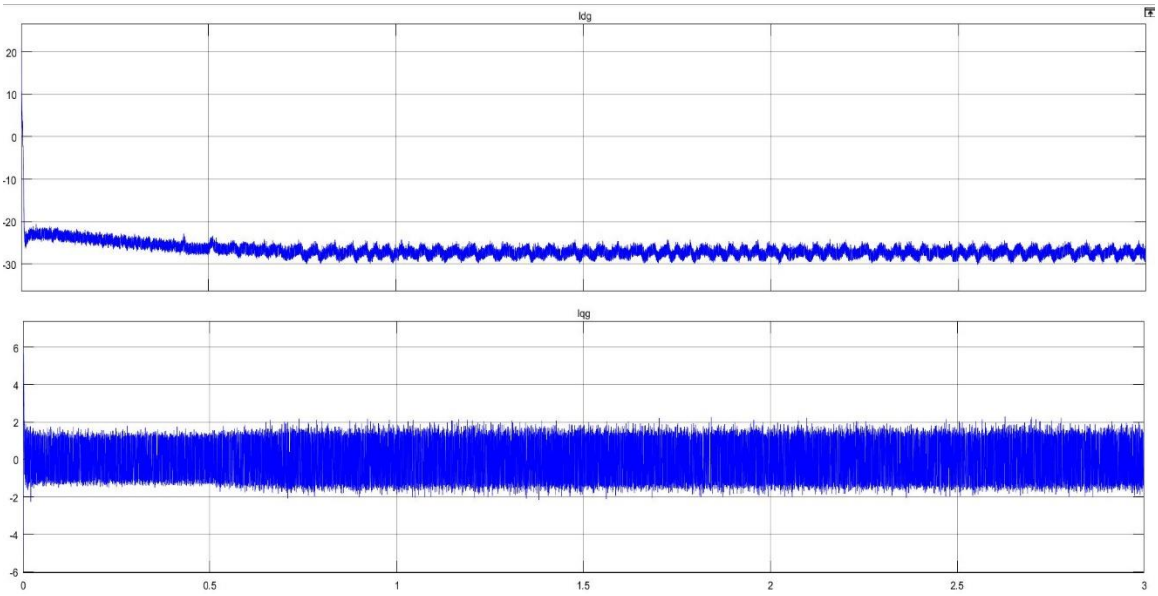


Figure 5-18 Measured d-axis current and q-axis current of the grid.

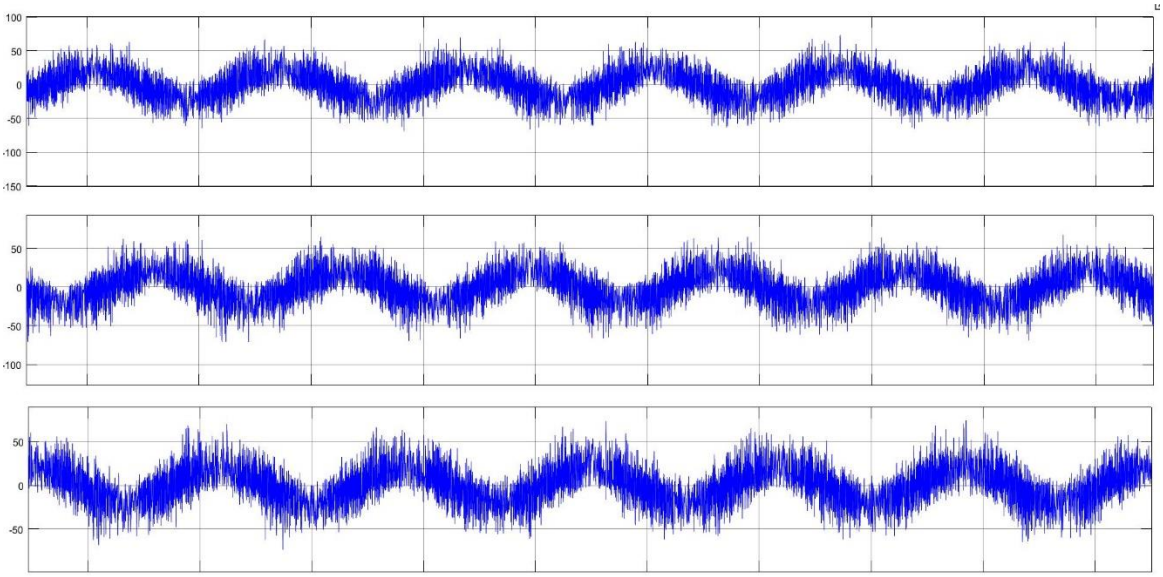

Figure 5-19 Three phase control voltage feeding to the PWM of the inverter with a 120$^{o}$ phase shift.

Grid side voltage and current are shown in figure and figure. The total harmonic distortion(THD) is also analyzed. The THD of voltage is 0.03% and the current THD is 3.64% at steady state.

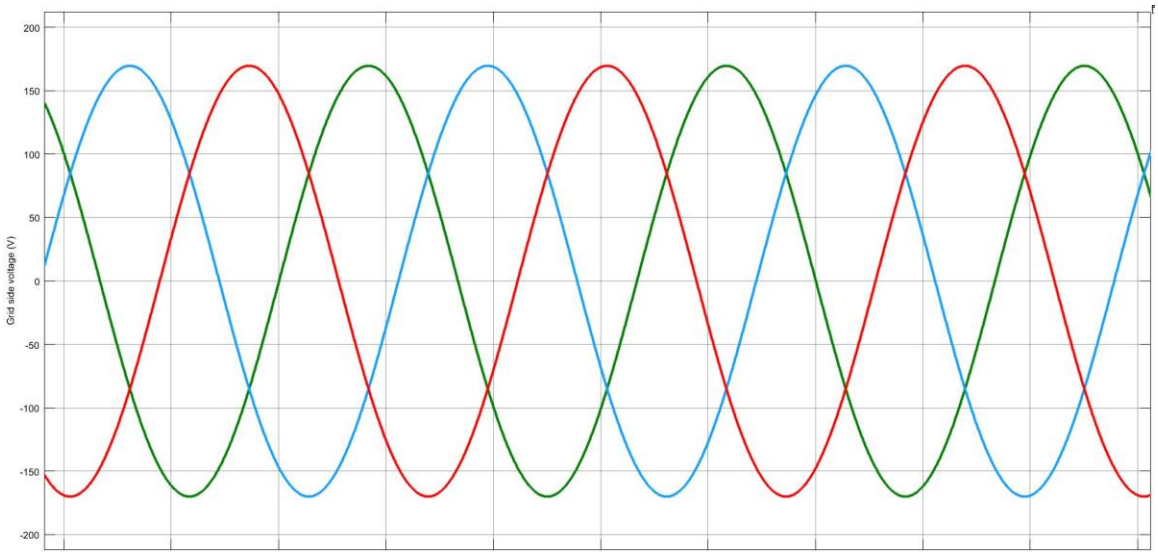


Figure 5-20 Grid side line to neutral voltage for phase a, b, and c.

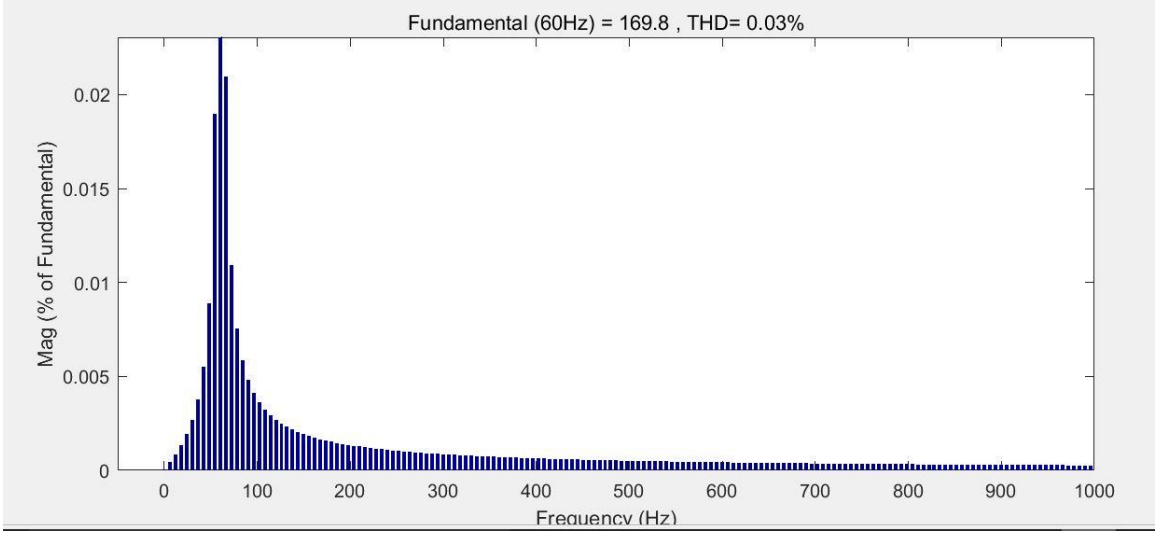


Figure 5-21 Grid side voltage THD given by FFT analysis.

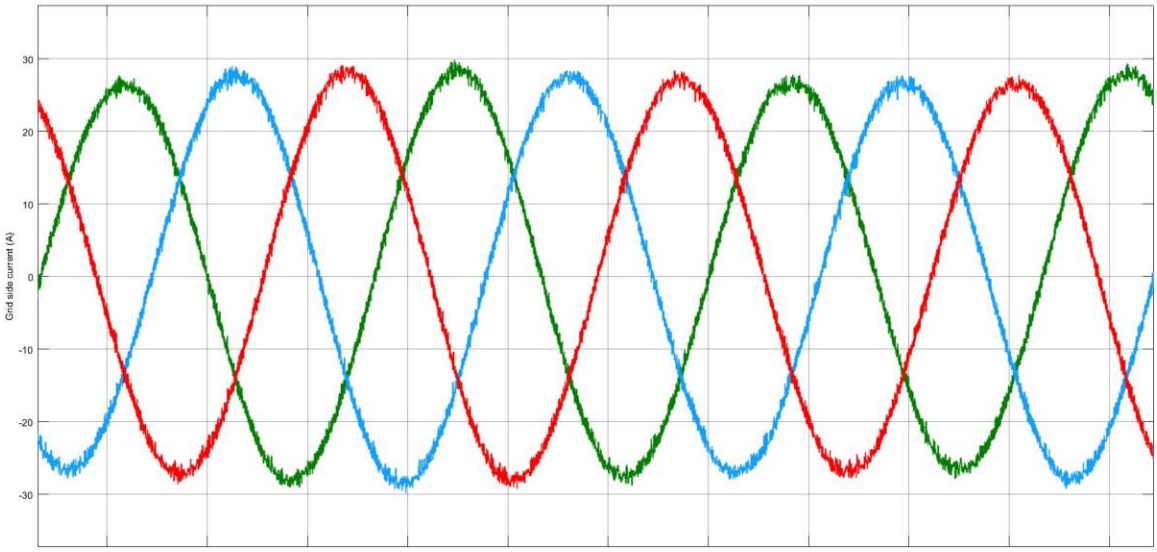


Figure 5-22 Grid side line to neutral current for phase a, b, and c.

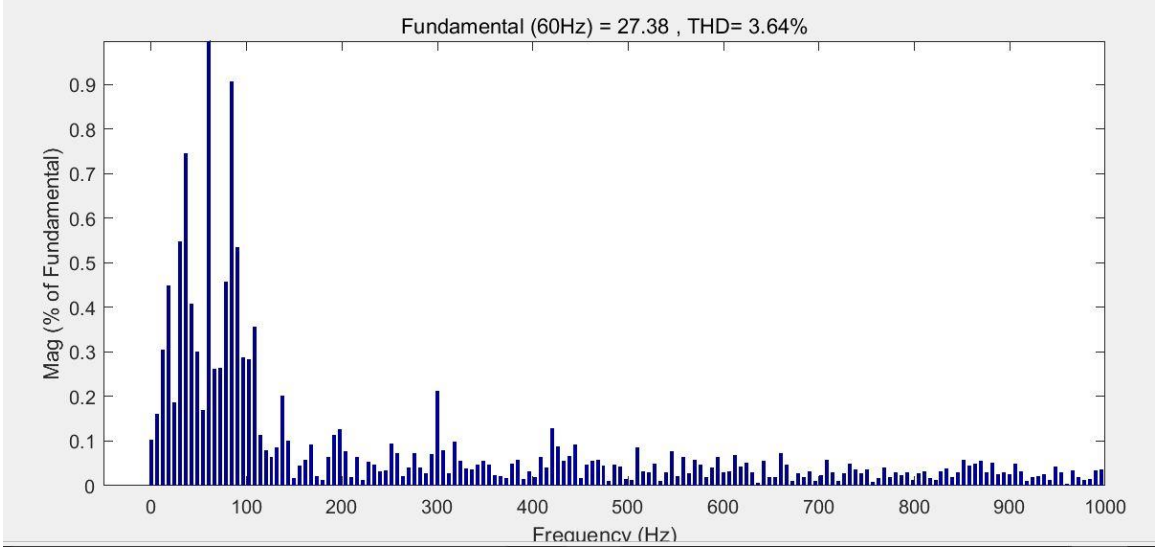


Figure 5-23 Grid side current THD given by FFT analysis.

## 5.2 Conclusion

The micro hydro turbine model is implemented to a AC/DC/AC power converter system with a P&O algorithm for MPPT. Unlike the traditional wind turbine system, the ideal generator speed is calculated irrespective to the nature circumstance and turbine parameters. Corresponding control strategy of boost converter and grid tie inverter are developed. The simulation is implemented in Matlab Simulink for the convenience of

working with both analog and digital devices. Also the PMSG model and IGBT switches can directly be selected from the Simpower library which save a lot of effect for building the model. The P&O algorithm can generate the ideal speed which matches the mechanical simulation result. The current loop control can maintain the PMSG speed at the reference value. The voltage oriented control can converter the power from the DC side to the AC side with an acceptable grid current THD. From the real-time scope of Simulink, we can clearly see the change of power as the generator speed varies for a low speed to the maximum power speed.

### 5.3 Future work

The hydro turbine model simulation result is based on a single head flow situation. More speed-power curve can be obtained under different head flow conditions are needed to verify the universality of the P&O algorithm for MPPT in such a model. Also, the micro hydro turbine model should be modeled into a general form which can express the power and torque relationship with respect to the speed under different circumstance. For the grid tie inverter, more complex filter topology like LCL filter can be implemented to the gird side and decrease the current THD and the size of the grid side inductor. Space vector modulation can also be developed for the inverter gate signal instead of the simple PWM topology.

# References


1. Renewable Energy Cost Analysis: Hydropower. (n.d.). Retrieved April 11, 2017, from https://www.bing.com/cr?IG=F37A4188C3684105BC145AEEDC8B4EC9&CID=38B0707D05506E0837567A1C04C06F9A&rd=1&h=Ic4EdCc1RTR7J-FP7Wx2lt-ghoX0s756hGS-Ti6Ngo8&v=1&r=https%3a%2f%2fwww.irena.org%2fDocumentDownloads%2fPublications%2fRE_Technologies_Cost_Analysis-HYDROPOWER.pdf&p=DevEx,5061.1

2. Microhydropower Systems. (n.d.). Retrieved April 11, 2017, from https://energy.gov/energysaver/microhydropower-systems

3. Planning a Microhydropower System. (n.d.). Retrieved April 11, 2017, from https://energy.gov/energysaver/planning-microhydropower-system

4. Tracking Progress - Renewable Energy. (n.d.). Retrieved April 11, 2017, from http://www.bing.com/cr?IG=E7BBFC7ED1C84C4D81C3B874AC9AF057&CID=03A3189718A26ECC09A012F619326F9F&rd=1&h=Bz9bnQPjQ5DDQe6BkMxUfc3dd34Bh0vS1XVAYC_qt10&v=1&r=http%3a%2f%2fenergy.ca.gov%2frenewables%2ftracking_progress%2fdocuments%2frenewable.pdf&p=DevEx,5062.1

5. M. Chinchilla, S. Arnaltes and J. C. Burgos, "Control of permanent-magnet generators applied to variable-speed wind-energy systems connected to the grid," in *IEEE Transactions on Energy Conversion*, vol. 21, no. 1, pp. 130-135, March 2006.

6. Teodorescu, R., Liserre, M., & Rodriguez, P. (2011). Grid converters for photovoltaic and wind power systems. Chichester: Wiley.

7. Indra, A. (2012, October 4). Industrial Fibre Optics In Wind Energy Applications. Retrieved March 08, 2017, from http://www.displayplus.net/news/articleView.html?idxno=39636

8. Siegfried Heier, "Grid Integration of Wind Energy Conversion Systems," John Wiley & Sons Ltd, 1998, ISBN 0-471-97143-X

9. About Microgrids. (n.d.). Retrieved April 11, 2017, from https://building-microgrid.lbl.gov/about-microgrids

10. Chakraborty, S., Simões, M. G., & Kramer, W. (2013). Power electronics for renewable and distributed energy systems: a sourcebook of topologies, control and integration. London: Springer.

11. N HYDROPOWER - International Energy Agency. (n.d.). Retrieved March 29, 2017,from:http://www.iea.org/publications/freepublications/publication/hydropower_essentials.pdf

12. Salles, Maurício B. C., Cardoso, José R., & Hameyer, Kay. (2011). Dynamic modeling of transverse flux permanent magnet generator for wind turbines. Journal of Microwaves, Optoelectronics and Electromagnetic Applications, 10(1), 95-105. https://dx.doi.org/10.1590/S2179-10742011000100010

13. MH in Nepal. (n.d.). Retrieved March 29, 2017, from http://microhydro.org.np/mh-in-nepal/'

14. Ensuring the Sustainability of Rural Electrification in Nepal. (n.d.). Retrieved March 29, 2017, from http://www.worldbank.org/en/news/feature/2015/09/26/ensuring-sustainable-rural-electrification-in-nepal

15. F. Blaabjerg, M. Liserre, and K. Ma, "Power electronics converters for wind turbine systems," IEEE Transactions on Industry Applications, vol. 48, no. 2, pp708-719, 2012

16. K. Samir, J. Rodriguez, B. Wu, S. Bernet, and M. Perez. "Powering the Future ofIndustry: High-Power Adjustable Speed Drive Topologies," Industry Applications Magazine, IEEE, vol. 18, no. 4 (2012): 26-39.

17. S. Kouro, M. Malinowski, K. Gopakumar, J. Pou, L. G. Franquelo, B.Wu,J. Rodriguez, M. A. Perez, and J. I. Leon, “Recent advances and industrial applications of multilevel converters,” IEEE Trans. Power Electron., vol. 57, no. 8, pp. 2553–2580, Aug. 2010.

18. D. S. Henderson and D. E. Macpherson, "Application of solid state switching devices to electronic load governing of micro hydro generators," 1993 Fifth European Conference on Power Electronics and Applications, Brighton, UK, 1993, pp. 244-249 vol.8.

19. N. P. A. Smith, "Induction generators for stand-alone micro-hydro systems," Proceedings of International Conference on Power Electronics, Drives and Energy Systems for Industrial Growth, New Delhi, 1996, pp. 669-673 vol.2.

20. D. Melly, R. Horta, C. Münch, H. Biner and S. Chevailler, "Development of a PM-generator for a counter-rotating micro-hydro turbine," 2014 International Conference on Electrical Machines (ICEM), Berlin, 2014, pp. 124-129.

21. Krishna Kumar M J, Vinod John, "Comparison of 3-phase, 3-level UPF Rectifier Circuits for High Power Applications", IEEE International Conference on Power Electronics, Drives and Energy Systems, Bengaluru, India, 2012.

22. K. T. Atta, A. Johansson, M. J. Cervantes and T. Gustafsson, "Maximum power point tracking for micro hydro power plants using extremum seeking control," 2015 IEEE Conference on Control Applications (CCA), Sydney, NSW, 2015, pp. 1874-1879.

23. R. C. Prajapati, D. Rai and B. B. Chhetri, "Economic and Simple Power Line Modem Design for the Utility Applications in Micro-Hydro Power Systems of Nepal," 2006 IEEE International Symposium on Power Line Communications and Its Applications, Orlando, FL, 2006, pp. 44-49.

24. Morimoto, S. (2007), Trend of permanent magnet synchronous machines. IEEJ Trans Elec Electron Eng, 2: 101–108. doi:10.1002/tee.20116

25. M. Singh, Adaptive Network-Based Fuzzy Inference Systems for Sensorless Controlof PMSG Based Wind Turbine With Power Quality Improvement Features. (Doctoral dissertation). Retrieved from ProQuest Dissertation and Thesis.

26. A. E. Fitgerald, J. C. Kingsley, and S. D. Umans, Electric Machinery. New York: McGraw-Hill, 1990.

27. V. Bobek, PMSM Electrical Parameters Measurement. Freescale Semiconductor Application Note. Document Number:AN4680 Rev. 0, 02/2013

28. Bedi, E. (n.d.). DIERET: Hydro. Retrieved April 03, 2017, from

http://www.inforse.org/europe/dieret/Hydro/hydro.html

29. A.L. Quilisch, *Object Oriented Modelling and Simulation of Kaplan Turbines,* Masters' Degree Project Stockholm, Sweden February 2008

30. Munson, B. R., Okiishi, T. H., & Young, D. F. (1999). Fundamentals of fluid mechanics. New York: Wiley.

31. Wind Resource: Utilising Hydrogen Buffering. (n.d.). Retrieved April 04, 2017, from http://www.esru.strath.ac.uk/EandE/Web_sites/08-09/Hydrogen_Buffering/Website%20Power%20Conditioning.html

32. Step Up Boost Regulator or Converter. (n.d.). Retrieved April 04, 2017, from http://www.radio-electronics.com/info/power-management/switching-mode-power-supply/step-up-boost-regulator-converter-basics.php

33. Erickson, R. W., & Maksimović, D. (2004). Fundamentals of power electronics. Dordrecht: Kluwer.

34. H. Abdel-Gawad and V. K. Sood, "Small-signal analysis of boost converter, including parasitics, operating in CCM," 2014 6th IEEE Power India International Conference (PIICON), Delhi, 2014, pp. 1-5.

35. R. Esmaili, L. Xu and D. K. Nichols, "A new control method of permanent magnet generator for maximum power tracking in wind turbine application," IEEE Power Engineering Society General Meeting, 2005, 2005, pp. 2090-2095 Vol. 3.

36. Mohan, N., .., M., Robbins, W. P., & Undeland, T. M. (1995). Power electronics: converters, applications, and design. New York, NY: Wiley.

37. W. (2016, March 29). Voltage Controlled Oscillator - Usage of VCO, Working and Application. Retrieved April 09, 2017, from https://www.elprocus.com/voltage-controlled-oscillator-working-application

38. D. C. Huynh, T. A. T. Nguyen, M. W. Dunnigan and M. A. Mueller, "Maximum power point tracking of solar photovoltaic panels using advanced perturbation and observation algorithm," 2013 IEEE 8th Conference on Industrial Electronics and Applications (ICIEA), Melbourne, VIC, 2013, pp. 864-869.

39. X. Liu and L. A. C. Lopes, "An improved perturbation and observation maximum power point tracking algorithm for PV arrays," 2004 IEEE 35th Annual Power Electronics Specialists Conference (IEEE Cat. No.04CH37551), 2004, pp. 2005-2010 Vol.3.

40. Arroyo, E. L. (2006). MODELING AND SIMULATION OF PERMANENT MAGNET SYNCHRONOUS ... Retrieved April 11, 2017, from http://www.bing.com/cr?IG=CBD9E002256F4B55A70A4C99BD2729CB&CID=0B11C7C3E511646C191CCDA1E48165E5&rd=1&h=3KTSPm6Mj6xVKKWgenww0u7cKe3jlNujd8TUkHCm4H4&v=1&r=http%3a%2f%2fwww.ieee.hr%2f_download%2frepository%2flres_tema5_2.pdf&p=DevEx,5061.1Master thesis